Understanding the influence of slag fineness and water-to-binder ratio on the alkali-silica reaction in alkali-activated slag mortars

Wang, Wei; Zhang, Shizhe; Zhang, Yamei; Noguchi, Takafumi; Maruyama, Ippei

DOI
10.1016/j.cemconcomp.2024.105907

Publication date
2024

Document Version
Final published version

Published in
Cement and Concrete Composites

Cement and Concrete Composites 157 (2025) 105907

Contents lists available at ScienceDirect

Cement and Concrete Composites

journal homepage: www.elsevier.com/locate/cemconcomp

Understanding the influence of slag fineness and water-to-binder ratio on the alkali-silica reaction in alkali-activated slag mortars

Wei Wang [a,b,*], Shizhe Zhang [c], Yamei Zhang [a], Takafumi Noguchi [b], Ippei Maruyama [b,d]

[a] Jiangsu Key Laboratory of Construction Materials, School of Materials Science and Engineering, Southeast University, Nanjing, 211189, PR China
[b] Building Materials Engineering Laboratory, Department of Architecture, Graduate School of Engineering, The University of Tokyo, Tokyo, 113-8654, Japan
[c] Microlab, Section Materials and Environment, Faculty of Civil Engineering and Geosciences, Delft University of Technology, Stevinweg 1, 2628 CN, Delft, the Netherlands
[d] Concrete Engineering Laboratory, Department of Environmental Engineering and Architecture, Graduate School of Environmental Studies, Nagoya University, Nagoya, 464-8601, Japan

ARTICLE INFO

Keywords:
Alkali-silica reaction
Alkali-activated materials
Mixture design
Mass change
Pessimum effect

ABSTRACT

The use of alkaline activator in alkali-activated materials (AAMs) may pose risk of alkali-silica reaction (ASR), and the variations in the mixture design could have great influence on the performance of AAMs system. In this case, this paper investigated the effects of slag fineness (3000–8000 cm^2/g) and water-to-binder (w/b) ratio (0.5–0.8) on ASR behavior of alkali-activated slag (AAS) mortars under accelerated mortar testing conditions as specified in ASTM C1260. The length change, mass gain, microstructure and formation of ASR products were examined to evaluate the degradation caused by ASR. It was found for the first time that slag fineness induces a "pessimum effect" in the ASR expansion of AAS mortars. On the other hand, there is a "pessimum effect" in the influence of w/b ratio on ASR expansion in the early-stage (≤14d), and the induced expansion increased with an increase in w/b ratio in the late-stage (>14d). The mechanism governing the effect of slag fineness and w/b ratio is complicated and cannot be explained solely by the properties of ASR products. This work contributes to the understanding of ASR in AAMs system and could provide a basis for the mixture optimization of AAMs.

1. Introduction

Alkali-activated materials (AAMs) as a promising alternative to Portland cement have been widely studied in these years in particular due to its lower energy consumption and carbon footprint [1–4]. Although the reaction products in AAMs are different from those formed after cement hydration, it has been considered by many researchers that AAMs have better mechanical properties [5,6], fire resistance [7] and so on [8,9]. However, the use of high-pH alkaline activator for AAMs may pose the risk of alkali-silica reaction (ASR) when mixed with reactive aggregate [10–14].

ASR is a chemical reaction between the amorphous or poorly crystallized silica in aggregates and hydroxide ions in the pore solution of a concrete [15]. The occurrence and damage caused by ASR can be influenced by many factors, including aggregate, binder, mixture design, exposure conditions and so on [16–22]. Up till now, some studies have investigated the risk of ASR in AAMs system [10–14,23–34]. However, due to the variations in testing methods, alkali-reactivity of aggregate and mixture design of AAMs, the results are far from conclusive and sometimes even contradictory [35,36]. Some studies reported that the ASR-induced expansion of AAMs system increased with alkali dosage [28,37], and others reported that the expansion decreased with alkali dosage [26]. Nonetheless, Shi et al. [12] conducted a comprehensive study on the influence of alkali dosage and silicate modulus on ASR in alkali-activated slag (AAS) mortars and found that the effect of alkali dosage on ASR expansion was affected by the silicate modulus. From these studies, it can be seen that the variation in mixture design could have great impact on the ASR performance of AAMs system. Therefore, it is important to further investigate the effect of internal factors of mixture on the ASR behavior in AAMs system.

Compared with ordinary Portland cement (OPC) system, AAMs have many parameters that need to be taken into account in mixture design [38,39]. Apart from the chemical composition of precursors and activators, the particle size of precursors and water-to-binder (w/b) ratio are

* Corresponding author. Jiangsu Key Laboratory of Construction Materials, School of Materials Science and Engineering, Southeast University, Nanjing, 211189, PR China.
E-mail address: wang-wei@seu.edu.cn (W. Wang).

https://doi.org/10.1016/j.cemconcomp.2024.105907
Received 19 June 2024; Received in revised form 5 December 2024; Accepted 17 December 2024
Available online 20 December 2024

also important factors which can largely influence the reaction and microstructural development of AAMs, especially in the early-age reaction [40,41]. Meanwhile, w/b ratio and particle size are parameters that can be easily changed in the mixture design. For OPC system, it has been reported that the particle size of supplementary cementitious materials (SCMs) has a significant influence in mitigating ASR [42–44], and w/b ratio is also an important factor affecting the ASR performance [17]. However, so far, no data is available in the literature for the effect of precursor fineness and w/b ratio on the ASR behavior of AAMs system. Furthermore, compared with OPC system, water plays a different role in AAMs system. Based on the hydration mechanism of OPC system, water is a main reactant and is critical for the hydration process of OPC system. For AAMs system, the variations of w/b ratio not only change the water content of the mixture but also change the concentration of alkali activator solution, which could influence the dissolution and precipitation stage of the activation, and thereby further alter the types and structures of the reaction products, as well as the reaction rate in the early-age [3,4]. In a recent study, Wang et al. [13] reported that the early-age reaction is important for the ASR in AAMs system. Therefore, considering the potential influence of precursor fineness and w/b ratio on early-age reaction of AAMs, it is essential to investigate the effect of fineness of binder and w/b ratio on the ASR performance in AAMs system to bridge the knowledge gap and further clarify the mechanism of ASR in AAMs system.

In this work, the main objective is to evaluate the effects of slag fineness and w/b ratio on ASR performance in AAMs system. To better understand the mechanism, the mechanical properties, length change, mass gain, microstructure and formation of ASR products were investigated and discussed.

2. Materials and methods

2.1. Materials

The solid precursor in this study is a commercial ground granulated blast-furnace slag (GGBFS), which conforms to Japanese industrial standard (JIS A6206) [45]. Four types of GGBFS with different fineness were used, which were labelled according to JIS A6206 and their specific surface area (3100 cm^2/g, 4040 cm^2/g, 5860 cm^2/g and 8020 cm^2/g) as S3000, S4000, S6000 and S8000, respectively. Their chemical compositions are shown in Table 1. The particle size distribution of different types of GGBFS are shown in Fig. 1. The median particle size (d_{50}) of the GGBFSs is 26.88 μm, 14.93 μm, 8.16 μm and 4.99 μm, respectively.

The activator used was water-glass with a silicate modulus of 1.5 (Ms = SiO_2/Na_2O by mass), which was prepared by modifying the commercial sodium silicate solution (Ms = 3, water content = 60 ± 1 %) with extra NaOH pellets (purity>98.5 %) and deionized water. In order to eliminate the influence of heat release during dilution on the experiment, the activator solutions were prepared one day prior to the mortar preparation to allow the cooling down of the solution.

Aggregate from Toyama prefecture in Japan was used as a reactive aggregate (RA) in this study, which was proved highly reactive in real OPC structures. Its chemical compositions are presented in Table 1, and mineral compositions are shown in Fig. 2. RA is composed of feldspar, cristobalite, biotite, clinochlore, richterite, and quartz with an amorphous content of approximately 34.7 wt% acquired by Rietveld refinement method. The size of aggregate was sieved to meet the requirements in standard ASTM C1260.

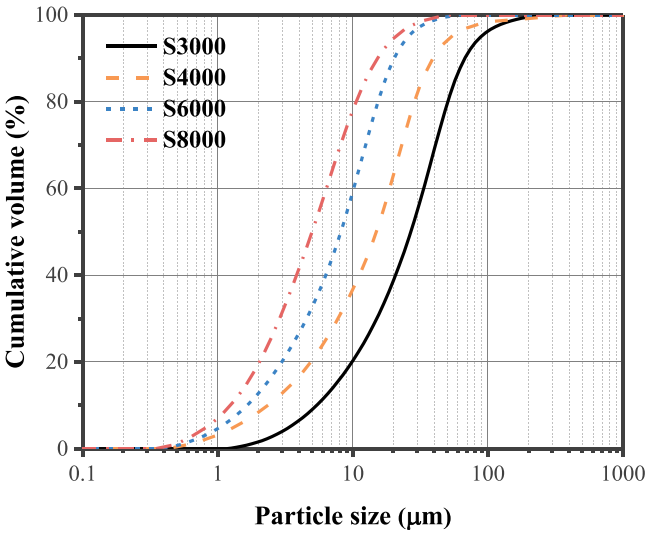

Fig. 1. Particle size distribution of GGBFS.

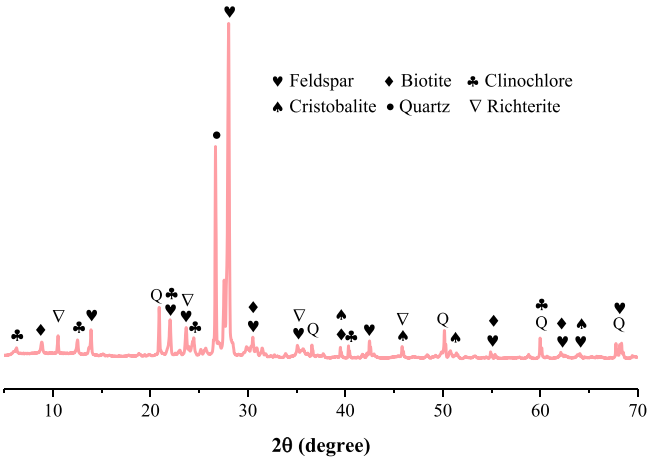

Fig. 2. XRD pattern of RA [14].

2.2. Mortar preparation

The mortar specimens (40mm × 40mm × 160 mm) with measuring pins embedded in both face sides were prepared as the mixtures shown in Table 2. The high water/binder ratio used in this study was designed to decrease the alkalinity to reduce the cost and causticity of AAMs with acceptable properties. After cured for 24 h within moulds in a climate chamber (T = 20 °C, RH = 95 %), the specimens were demoulded and

Table 1
Chemical composition of GGBFS and RA (wt %) [14].

Ingredients	CaO	SiO_2	Al_2O_3	Fe_2O_3	MgO	Na_2O	K_2O	SO_3	Na_2Oeq	LOI
S3000	43.63	31.07	12.40	0.32	5.45	0.25	0.34	1.85	0.47	0.37
S4000	42.91	31.42	13.54	0.33	6.04	0.30	0.32	1.52	0.51	0.33
S6000	43.16	31.43	12.92	0.26	5.85	0.29	0.29	1.23	0.48	0.41
S8000	43.51	31.23	12.94	0.28	5.74	0.27	0.31	1.44	0.47	0.40
RA	4.87	58.97	17.28	12.02	2.02	0.71	1.79	–	1.89	0.89

Note: $Na_2Oeq = \%Na_2O + 0.658\%K_2O$.

Table 2
Mixture proportions of mortars.

Sample ID	Binder	Alkali dosage	Silicate modulus	Aggregate/binder	Water/binder
AAS3000	S3000	6 % Na_2O by weight of binder	1.5	2.25	0.5
AAS4000	S4000				0.5
AAS6000	S6000				0.5
AAS8000/AAS8000–0.5	S8000				0.5
AAS8000–0.6	S8000				0.6
AAS8000–0.7	S8000				0.7
AAS8000–0.8	S8000				0.8

Note: AAS8000–0.6 represents the AAS mortar prepared with GGBFS8000 at a water-to-binder ratio of 0.6.

then transferred into a steam chamber (T = 80 °C) for 22 h initial curing. Afterwards, the specimens were immersed into 1 mol/L NaOH solution at the same steam chamber for 2 h [12,46], which is conformed to ASTM C1260.

2.3. Testing methods

2.3.1. Compressive strength and elastic modulus

The compressive strength and elastic modulus test were performed on sealed cured (20 °C) cylinder paste specimens (Φ50 × 100 mm) in agreement with JIS R5201 [47] and JIS A1149 [48] at 1, 3, 7, and 28 days. Each reported value represents the mean of three replicate results.

2.3.2. Length and mass change measurement

After initial curing and immersion in 1 mol/L NaOH solution (80 °C) for 2 h [12,27], the specimens were removed from the chamber. This step was modified from ASTM C1260 to reduce alkali leaching [46]. The initial length of the mortar bars, commonly referred to as the "zero reading", were then measured using a digital gauge meter with a precision of 0.001 mm. Then, the specimens were immersed into 1 mol/L NaOH solution (80 °C) for 80 days. The average length of the mortar bars was reported based on the results of three replicates on each designated testing age.

To monitor the mass change of mortar specimens during the exposure time, the mass of specimens (surface wiped with cloth) was weighted by using an electronic balance after the length measurement.

2.3.3. QXRD analysis

XRD analysis was performed using a Rigaku-Mini Flex 600 X-ray diffractometer on the paste and mortar samples after 80 days exposure. The specimens were crushed into small pieces and submerged in isopropanol to stop hydration. The resultant dried samples were further powdered using an agate mortar until passing through a 63 μm sieve. The process of samples preparation followed the procedures in Ref. [49], and the equipment's operating conditions were CuKα X-rays with a step size of 0.020° and a scanning rate of 2°/min, ranging from 5° to 70°. The internal standard method was adopted, 10 mass% of alpha-corundum was mixed with 90 mass% of mortars powder and the samples were manually mixed further for 10 min to get homogeneous samples.

2.3.4. MIP analysis

MIP analysis was performed on pastes sealed cured for 28 days (dried using the solvent exchange method [49]) using a Micromeritics AutoPore V 9600. The range of intruding pressure of this machine is from 1.379 kPa to 227.53 MPa, the surface tension of mercury is 0.485 N/m and the contact angle is 130°, respectively. According to the Washburn equation [50], the pore radius can be detected ranges from 0.005 μm to 800 μm.

2.3.5. SEM/EDS observation

Scanning Electron Microscopy (SEM) and Energy Dispersive X-ray Spectroscopy (EDS) analysis were conducted using a JEOL JSM-7800F microscope on specific mortar samples. The acceleration voltage applied in the experiment was 15 kV, and the operational distance was 10.0 mm. The EDS counting procedure was conducted using a highly accurate automated model, with the duration of the acquisition being determined by the count quantity of 250,000. After an 80-day period of exposure and mass measurement, the mortar specimens underwent slicing via a low-speed saw, with isopropanol serving as a lubricant. Then, the sliced samples were impregnated with a low-viscosity epoxy resin of low viscosity, and the polishing methodology was executed in accordance with the guidelines outlined in literature [49]. Before testing, all samples were Osmium coated to increase the electrical conductivity.

3. Results and discussion

3.1. Effect of slag fineness on ASR in AAS mortars

3.1.1. Mechanical properties of pastes

The compressive strength and elastic modulus development of AAS pastes with different GGBFS fineness is given in Fig. 3. It can be seen that the fineness of GGBFS has significant influence on the compressive strength and elastic modulus development. At the early age (1d and 7d), the strength of specimens increased with the increasing of fineness, while the strength of AAS8000 is lower than that of AAS6000 pastes at 28d.

In addition, it is interesting to find that the slag fineness has limited effect on the elastic modulus at 7d and 28d. When the slag fineness increased from 3000 to 8000 cm^2/g, the elastic modulus of AAS at 7d increased from 17.1 GPa to 18.5 GPa (an 8.0 % increase). This might be due to the development of shrinkage induced microcracking, and the shrinkage would increase with the increase of slag fineness [51,52]. Moreover, elastic modulus is known to be more sensitive to the influence of microcracking than compressive strength [51–54]. As shown in Fig. A1 (Appendix A), obvious shrinkage-induced cracks were observed on the surface of AAS8000 specimens, which is in agreement with the previous studies [40,55–57]. While there are arguments that MIP may not accurately represent the true pore size distribution of a material due to variations in pore shape and the "ink-bottle" effect, it can still provide insights into the differences in pore structure between equally prepared samples [58–60]. The pore structures of AAS pastes with different slag fineness after 28d is given in Fig. 4, where the volume of large size pores (>200 μm) could be as a result of gaps, the shrinkage-induced cracks or voids. Although it is not the traditional pore structure of AAMs, such kind of microstructure might be important for the development of ASR-induced expansion. The porosity and fraction of pores larger than 200 nm of AAS8000 pastes were higher than that of AAS6000 pastes, and the compressive strength is strongly dependent on the capillary porosity in AAM [61]. In this case, it suggests that there was an optimum fineness of slag in terms of strength. Meanwhile, these phenomena illustrate that the higher fineness of slag can accelerate the early-age reaction of AAS. Fast hydration could lead to quick consumption of water and lack of water for filling pores [62]. Due to high water demand of fast early-age reaction, the resulting shrinkage may decrease the mechanical properties of AAS in the long-term, which should be taken into account when choosing the fineness of GGBFS in practical use.

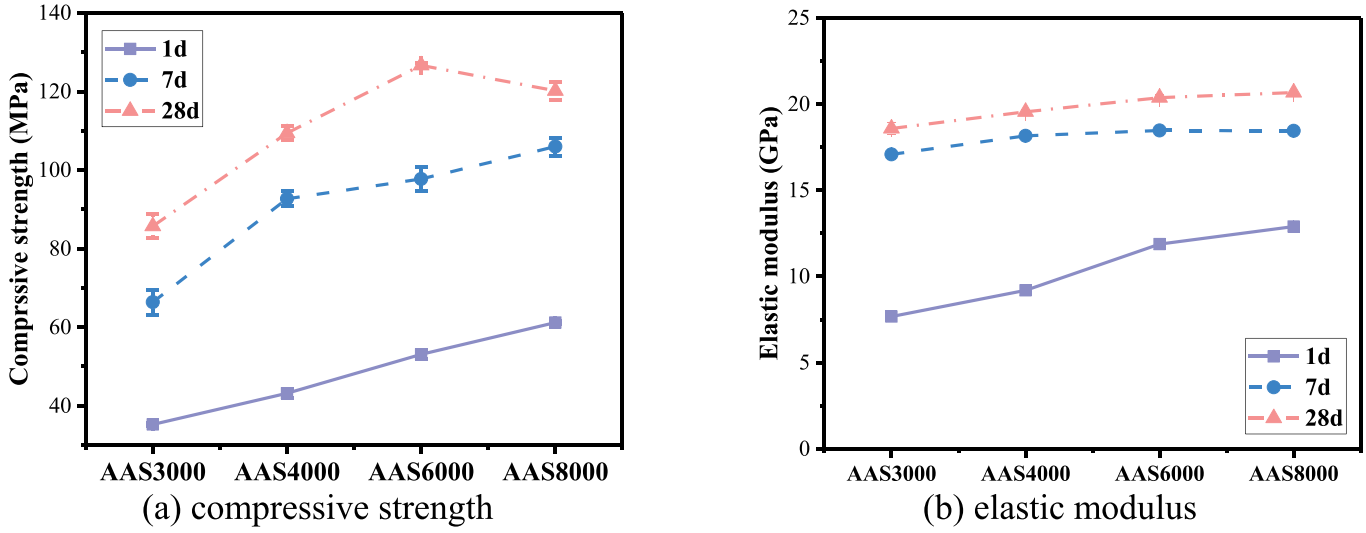

Fig. 3. Mechanical properties development of AAS pastes with different slag fineness.

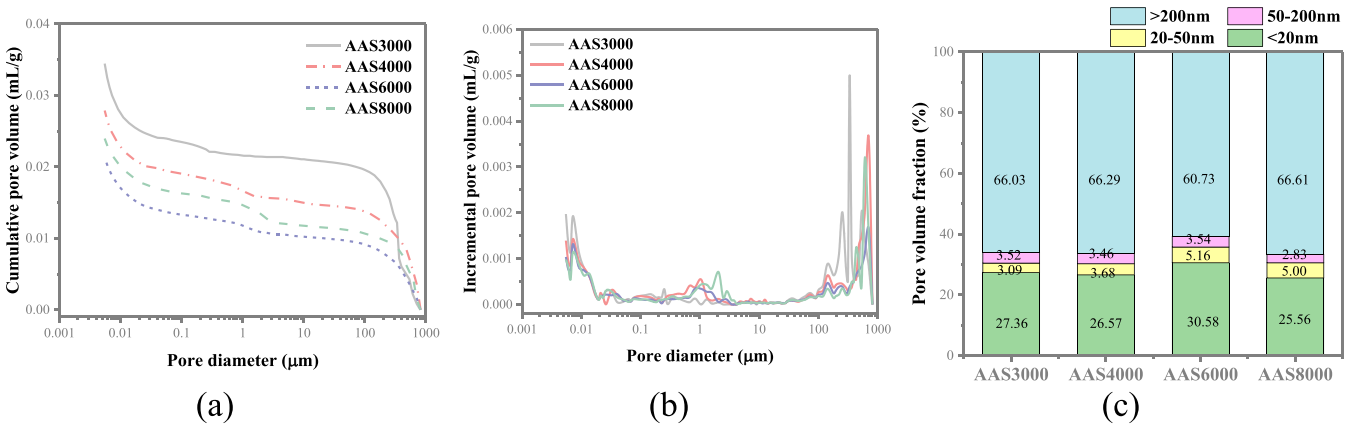

Fig. 4. Pore structure of AAS pastes with different slag fineness after 28d sealed curing.

3.1.2. Mortar bar expansion

The expansion evolution of AAS mortar bars with different slag fineness is shown in Fig. 5. The expansion of AAS mortars increased with time. With an increase in slag fineness, the expansion of AAS mortars increased first and then decreased, and this trend maintained throughout the exposure time (80 days). Moreover, the expansion of AAS4000 mortars still has a large potential to increase. It seems that there is a "pessimum effect" of slag fineness on the expansion development, which is similar with the classic pessimum effect of aggregate size on ASR in OPC system [63–67]. Currently, there is no data available on this subject in AAM so far. These performances are different from that of OPC system. Generally, in the OPC system, the finer supplementary cementitious materials (SCMs) could have a higher effectiveness in suppressing the ASR, as it can increase the reactivity and fasten the pozzolanic reaction of SCMs, and thereby decrease the pH and alkalis in the pore solution, which is critical for the ASR [42,44]. In AAMs system, the mechanism behind these phenomena becomes more complicated. The "pessimum effect" arises from a delicate balance of multiple parameters. On one hand, the higher strength and shrinkage of AAS6000 and AAS8000 could restrict the stress and diminish the expansion partly. Moreover, there is a competition between the reaction of slag and reactive silica in reactive aggregate. Slag with higher fineness react faster with the activator at the early age, which is confirmed by the more rapid strength development in section 3.1. The fast dissolution of slag at the early age decreased the pH and increase the dissolved Al and Si species from slag into the pore solutions, which could inhibit the dissolution of reactive silica from reactive aggregates [68–73]. In that case, both the amount of early-stage ASR gel and the osmotic pressure between the ASR gel and pore solution reduced. This reduction leads to a decrease in water uptake of ASR gel, and thereby reduced the long-term expansion. On the other hand, the consumption of reactive silica in reactive aggregates in the early-age reaction of AAMs, according to our previous study, could have a strong effect on the long-term ASR behavior of AAMs [13]. The finer slag accelerated the alkali-activation and reduce the dissolution and consumption of reactive silica in the RA at the early-age, and more reactive silica at the surface of RA is preserved, which could be supplied for ASR rather than consumed early-age alkali-activation. Previous studies have suggested that feldspar in RA contributes most to the ASR [13,19], and as shown in Fig. 6, with an increase in slag fineness, the feldspar content in AAS mortars increased. Consequently, the "pessimum effect" of slag fineness on the ASR-induced expansion of AAS mortars was due to a combination of reaction rate of slag, porosity, shrinkage, strength, amount of dissolved reactive silica from aggregates, and the competition between the reaction of slag and reactive silica as well as the amount of ASR gel and alkalis bound in the ASR gel. Further discussions will be given in Section 3.3.

3.1.3. Mass change

The mass change of AAS mortars with different slag fineness is shown

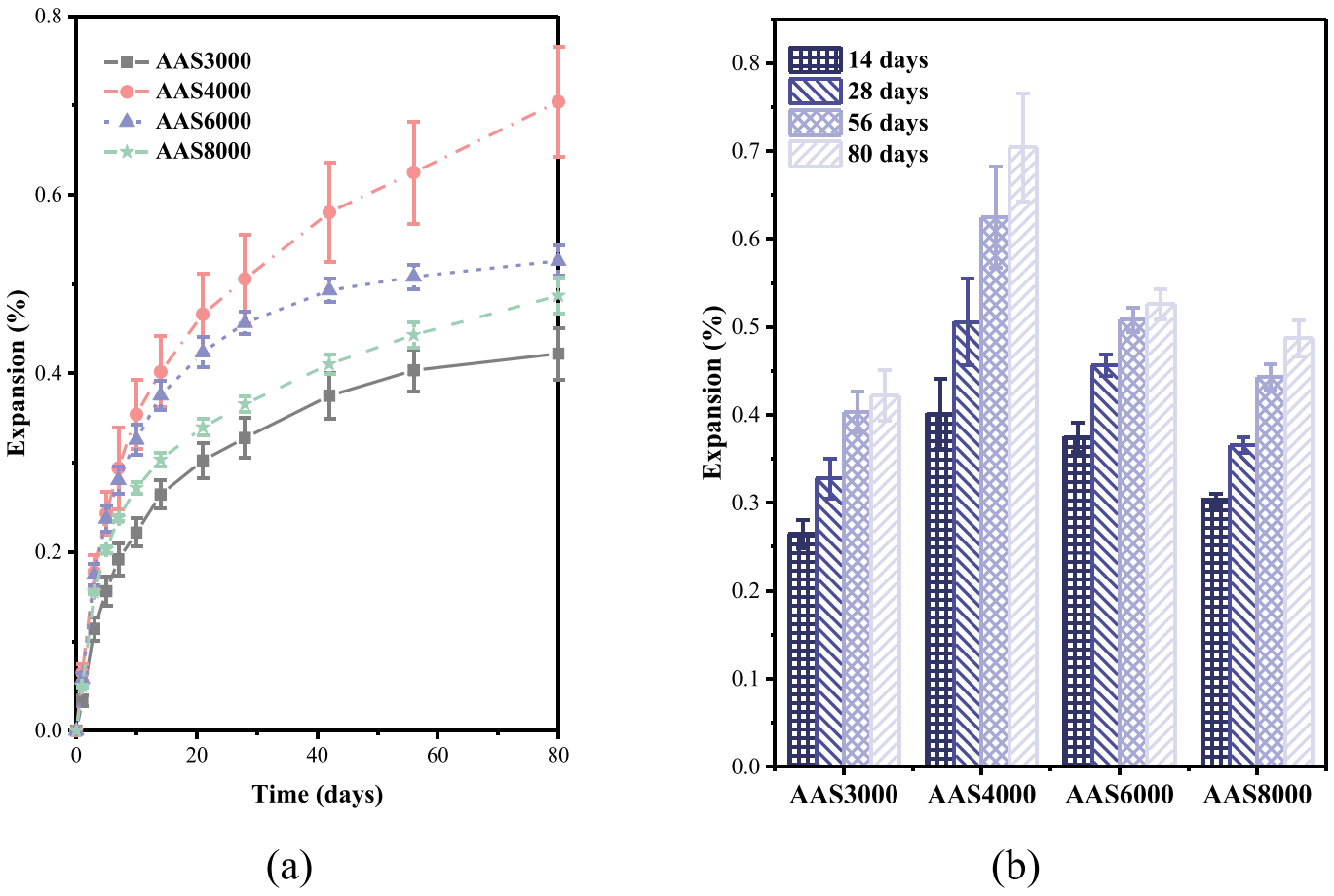

Fig. 5. (a) Expansion development of AAS mortars with different slag fineness; (b) Effect of fineness on the expansion AAS mortars after 14, 28, 56, and 80 days exposure.

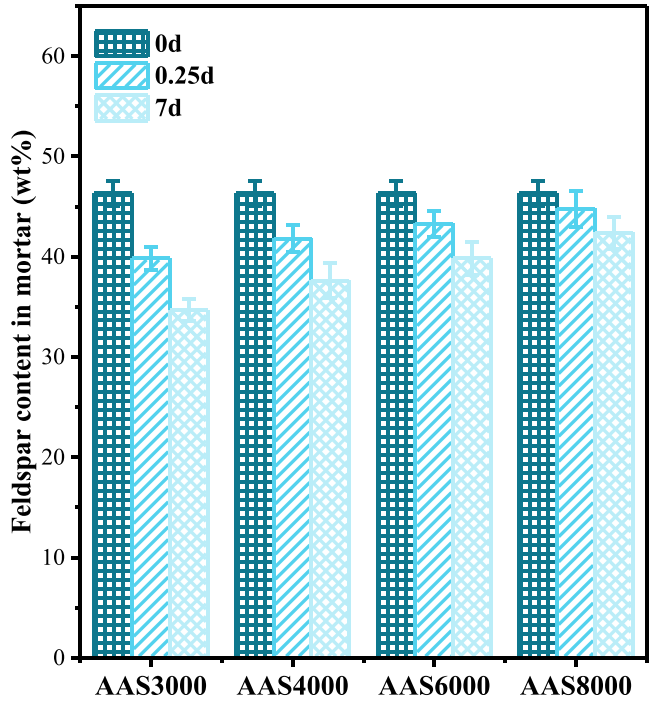

Fig. 6. Feldspar content in AAS mortars with different slag fineness.

in Fig. 7. The results show that the mass of mortars increased with increasing slag fineness, and all curves trend gradually to plateau. This may suggest that the continuous growth of expansion is a result of initial cracks development instead of continuous formation of more ASR products. The mass increase of mortars is mainly due to the binding of alkalis and water in the 1 mol/L NaOH solution in the generation of ASR products and further reaction of unreacted slag. Compared with the trend shown in Fig. 5, the similar trend could be found in the mass increase of AAS3000, AAS6000 and AAS8000 mortars, while the moderate mass gain of AAS4000 mortars exhibited the highest expansion. Meanwhile, with an increase in slag fineness, the feldspar content in AAS mortars increased (Fig. 6), which might mean the ASR products decreased (Feldspar is the main phase of the used reactive aggregate, which could be easily measured and judged. Therefore, it was used as an indicator of ASR.). This indicates that the mass gain of the mortars is not only controlled by formation of ASR products but also affected by the activation of unreacted slag. In the same concentration of extra alkalis, the finer of the particle size of slag, the easier and faster of alkali-activation of unreacted slag. In that case, the contribution of continued activation of unreacted slag for the mass gain is higher in AAS mortars using finer slag, and thereby the mass gain of AAS6000 and AAS8000 mortars are higher than that of AAS4000 mortars. This might also suggest that the amount of ASR products is much less, but the little ASR products could result in big expansion, which agrees with previous studies [27].

3.1.4. *Microstructure and chemical composition*

Representative backscatter electron (BSE) micrographs of polished samples after 80 days exposure is given in Fig. 8. ASR products could be

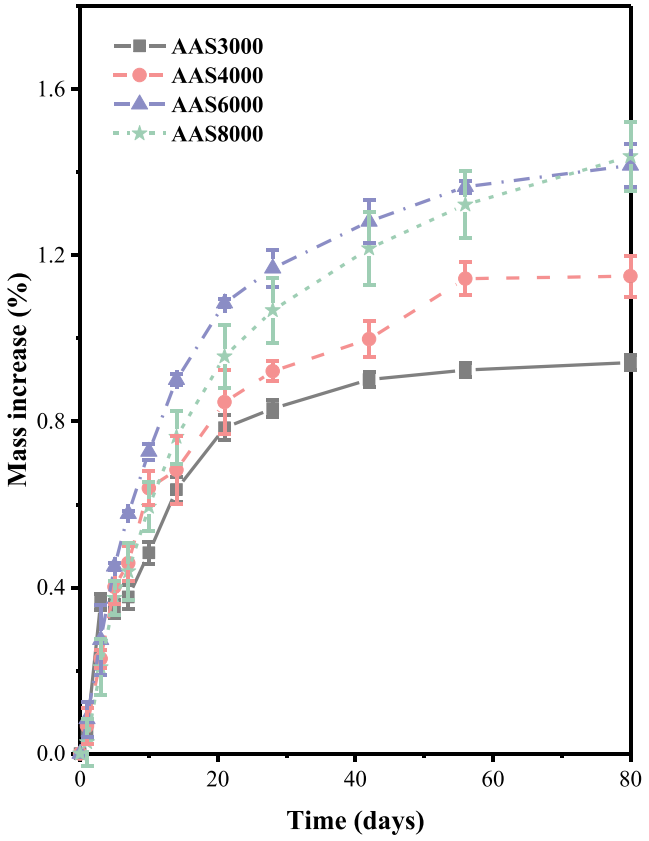

Fig. 7. Effect of slag fineness on the mass gain of AAS mortars.

easily observed in all samples. The difference is that there are many pores were left behind in the ASR products vein of AAS6000 and AAS8000 mortars. This phenomenon may suggest that the ASR products in AAS6000 and AAS8000 mortars are lower in the viscosity and easy to flow out. Previous studies [74,75] found that the viscosity of ASR products was largely dependent on its chemical composition. The lower calcium content and higher alkali content within an ASR product, the lower is its viscosity. To further confirm this hypothesis, the EDS analysis was conducted, and the results are shown in Fig. 9. As indicated, the calcium content of ASR products in AAS4000 mortars was relatively higher than that of other samples, while the sodium content was higher in AAS6000 and AAS8000 mortars, which explained that why the ASR products in the two mortars were easily flowed out and left the pores behind as well as the macro-expansion was lower than that of AAS4000 mortars. Therefore, the difference in the calcium and alkali content of ASR products in the corresponding samples might be affected not only by the initial ASR before cracking but also the interacting with the matrix after cracking. After cracking, the ASR products formed on the surface of aggregates are extruded into the matrix and filled the cracks or pores, increasing its Ca/Si by taking up calcium [76]. As discussed in section 3.1.2, the fast reaction of AAS6000 and AAS8000 might consume rapidly thus also more OH^- and Ca^{2+} ions in the pore solution and result in the low calcium concentration remained for the following increase of Ca/Si of ASR products. In that case, the crystallinity of ASR products in AAS6000 and AAS8000 is thereby low. Nevertheless, the crystallization pressure might be an additional mechanism of the stress generation and resultant expansion [76,77].

Besides, it should be mentioned that it is easier to find the ASR products in AAS4000 mortars, which implied a higher amount of ASR products was formed and consistent with the big expansion of AAS4000 in Fig. 5. The EDS elemental mapping of AAS4000 shown in Fig. 10 also suggests that the ASR products have higher Na, Si and K content, while lower Ca and Al content than that of the matrix, which is consistent with the previous studies on ASR in OPC system [17,19]. Such kind of differences could favor the osmotic pressure and ion exchange of ASR products.

3.2. Effect of water-to-binder ratio on the ASR in AAS mortars

3.2.1. Mechanical properties of pastes

The compressive strength and elastic modulus development of AAS pastes with different w/b ratio is given in Fig. 11. It can be seen that w/b ratio has significant influence on both the compressive strength and elastic modulus of specimens. With increasing w/b ratio, both the compressive strength and elastic modulus of AAS pastes decreased significantly at 1, 3 and 28 days. When the w/b ratio increased from 0.5 to 0.8, the compressive strength at 28 days decreased from 120.2 MPa to 60.1 MPa (a 50.0 % reduction), and the elastic modulus declined from 20.7 GPa to 13.5 GPa (a 34.9 % reduction). This reduction might be attributed to the dilution of activator with increasing of w/b ratio. In this way, both the alkalinity and the concentration of activator decreased, and thereby slow down the alkaline activation and as well as the formation of reaction products. Furthermore, the increase of w/b ratio also decreased the binder-to-volume ratio of the specimens, which is the binder content in the fixed volume of specimens, and thereby decreased binder content in the specimens and increased the porosity. Therefore, the mechanical properties were greatly sensitive to the variations of w/b ratio. As shown in Fig. 12, the porosity of specimens increased with w/b ratio, and it is noted that the nano-porosity (within the range of 5–20 nm pore size) of AAS8000–0.8 pastes is very high. Based on the relationship between pore structure and shrinkage [78–80], it implies that the shrinkage of AAS pastes decreased with increasing w/b ratio.

3.2.2. Mortar bar expansion

Fig. 13 shows the expansion evolution of AAS mortar bars with different w/b ratio. It can be seen that the expansion of AAS mortars increased with time. Furthermore, with an increase in w/b ratio, the expansion of AAS mortars increased first and then decreased in the early age (<28 days). In the later age (>80 days), the expansion of AAS mortars increased with the increasing of w/b ratio. Moreover, the expansion rate of AAS8000–0.7 and AAS8000–0.8 mortars was higher than that of AAS8000–0.5 and AAS8000–0.6 mortars in the later-age. These phenomena may be attributed to the balance between the rate and amount of gel formation, the viscosity of the gel, the porosity of the mortars and the confinement pressure, which will be further discussed in section 3.3.2.

In the early-age, the damage caused by the ASR-induced expansion was limited and the ASR products was well restrained, therefore, the expansion rate was mainly dependent on the reaction kinetics of ASR product formation. On the one hand, the lower alkaline activator with higher w/b ratio leads to lower pH of the pore solution and thereby reduced the reaction kinetics of not only the alkali activation of the binder but also the ASR. Furthermore, the compatibility between the formation of C-A-S-H and N-A-S-H gel also largely depends on the pH [81]. In that case, the decreased pH may favor the formation of ASR products. On the other hand, high w/b ratio increased the porosity of mortars and thus provide accommodation for part of ASR products. This help to alleviate the internal stress building up due to the formation of ASR products. Therefore, the induced expansion in the early-age is dependent on the balance between the rate of ASR products formation and the accommodations for ASR products provided by the porosity of the mortars, as well as the development of visco-elastic properties of the matrix. Besides, the shrinkage of the matrix may also play a vital role in compensating the expansion in the early stage, although it falls already outside the scope of this study.

In the later-age (after 7 days), as the reaction continued, the pH of AAS mortars decreased rapidly and the difference in alkalis concentration of mortars with different w/b ratio should be weakened [68,70–72].

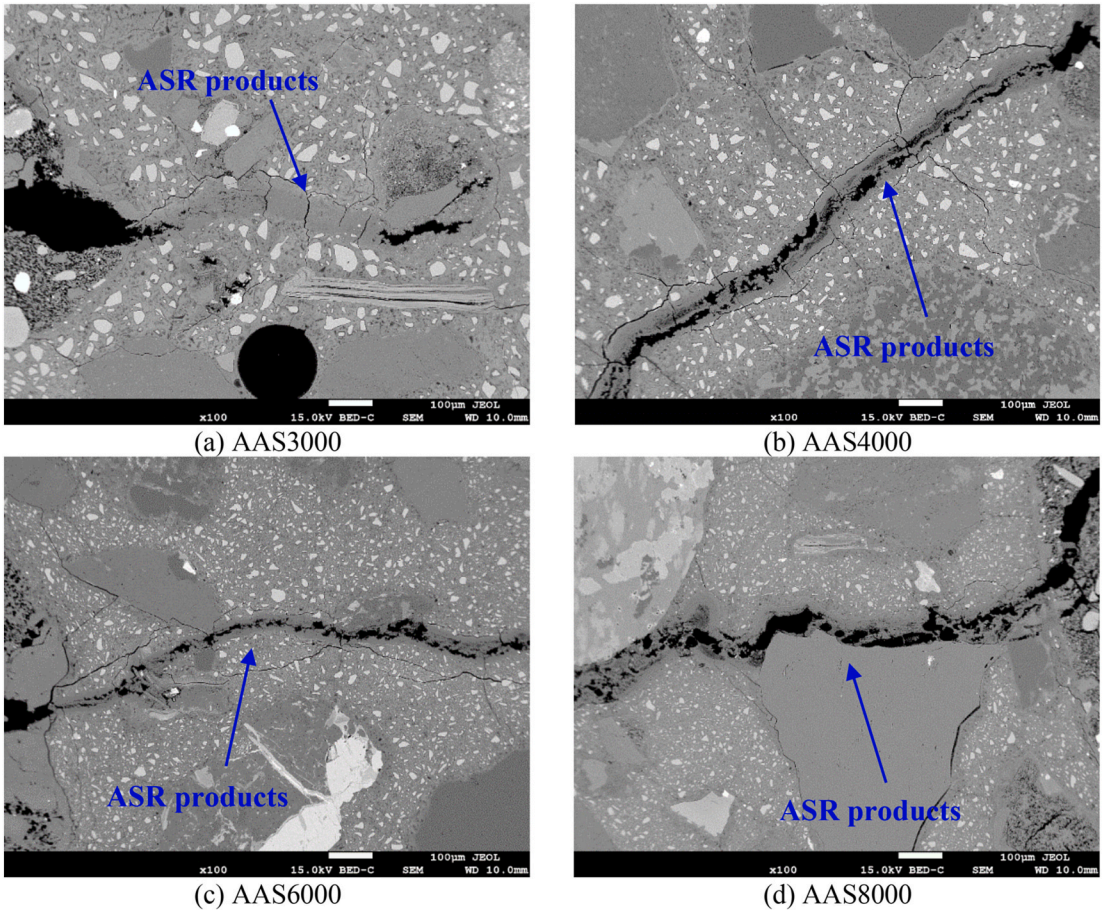

Fig. 8. Representative BSE images of mortar specimens with different slag fineness after 80 days of AMBT.

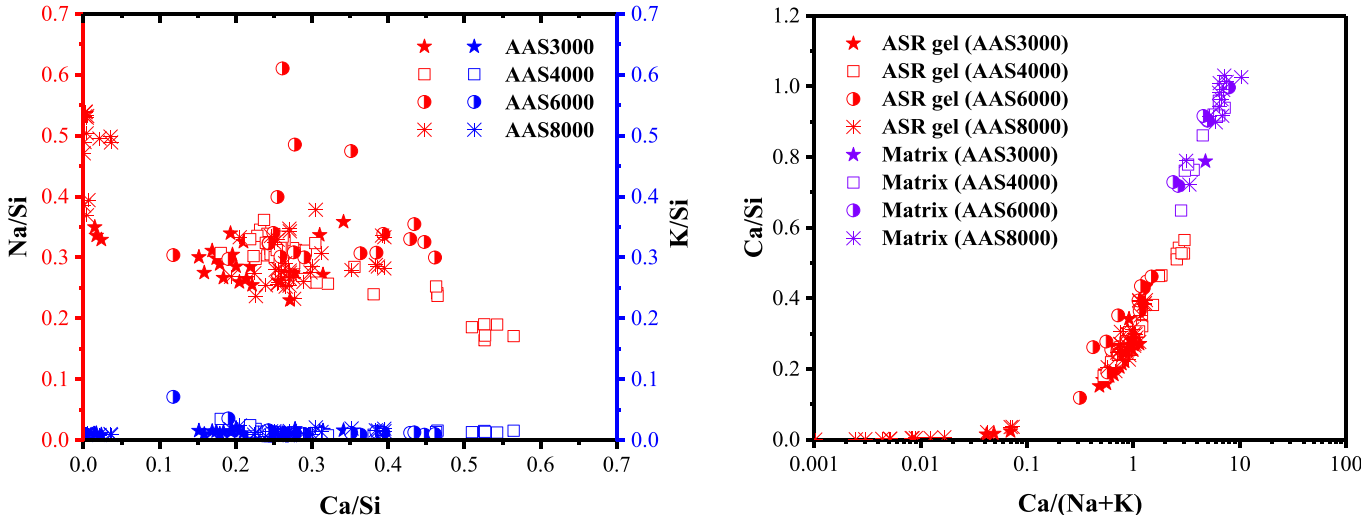

Fig. 9. Chemical composition (atomic ratio) of ASR products and matrix of AAS mortars.

Meanwhile, in this stage, the damage is expected to extend also into the matrix of the mortars. In this case, the expansion rate mainly depended on the amount of reactive silica in aggregates, confinement pressure provided by the matrix and the properties of the ASR products, as well as the development of the initial cracks. Regarding the formation rate of ASR products, due to the reduced difference in alkalis content [12,26], the rate is mainly influenced by the amount of reactive silica. According to our previous study [13], the reactive silica dissolved and consumed in the early-age reaction of corresponding AAS mortars is critical for the ASR behavior in AAMs system. With an increase in w/b ratio, the concentration of OH^- and alkalis decreased, hence, the dissolution and consumption of reactive silica in the early-age reaction of AAS mortars was retarded, leaving more silica for the later ASR products formation as given in Fig. 14. Besides, since the pastes with higher w/b ratio have in general lower mechanical properties, the confinement pressure provided by the matrix was also lower. Therefore, the initial cracking and further

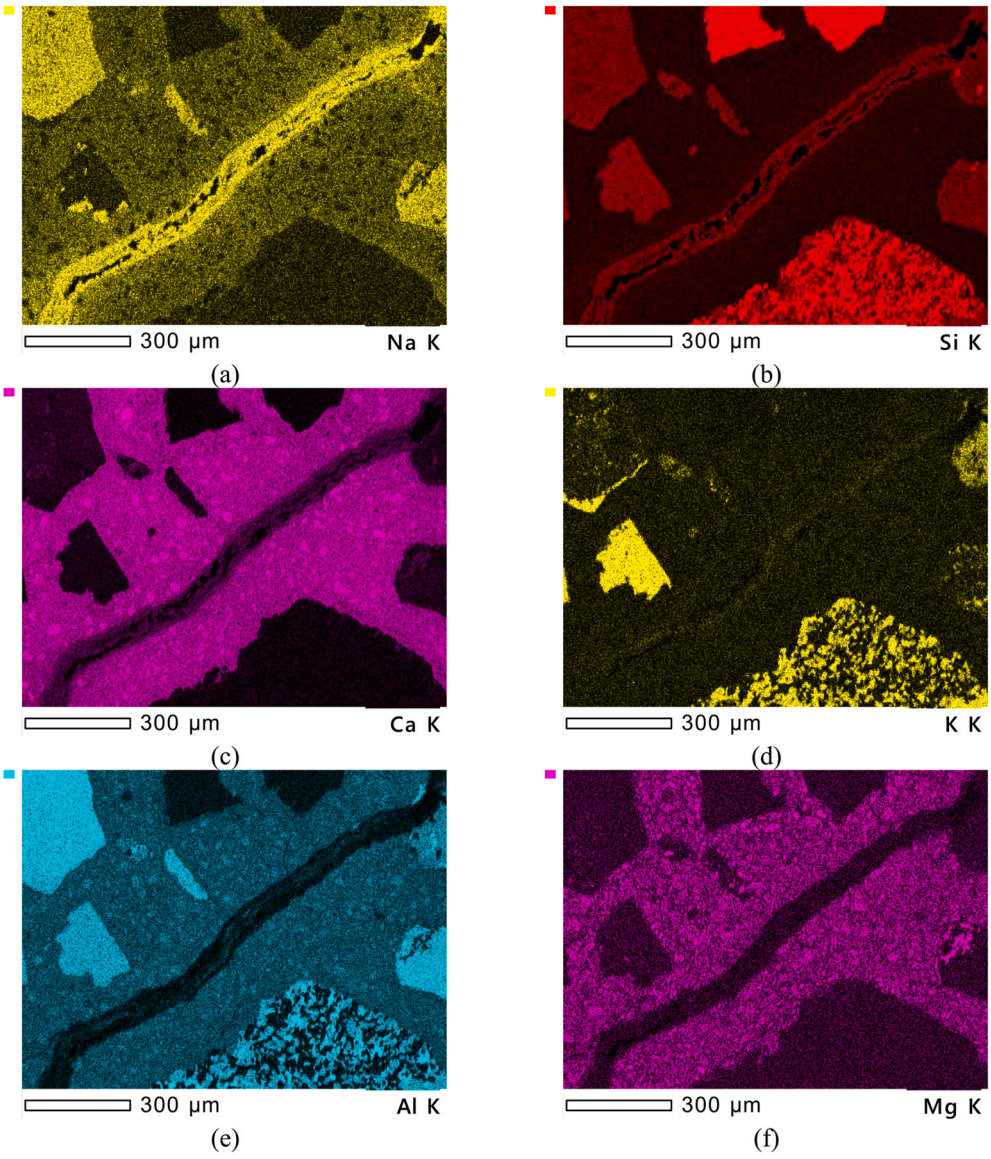

Fig. 10. EDS elemental mapping of ASR products in the AAS4000 mortars.

crack propagation in the matrix due to the ASR products can happen more easily. As a result, the AAS mortars with high w/b ratio showed a larger expansion due to ASR.

3.2.3. Mass change

The mass gain of AAS mortars with different w/b ratio is shown in Fig. 15. Similar to discussion made in Section 3.1.3, the mass gain of mortars could be attributed to the water uptake and alkalis binding of further reaction of unreacted binder and formation of ASR products. Different from the trend of expansion given in Fig. 13, the mass gain of AAS8000–0.5 mortars was higher than that of AAS8000–0.6 and AAS8000–0.7 mortars. This might be due to the early age shrinkage-induced micro-cracks, which provides access for the alkaline activator to the unreacted slag and thereby promoted the further alkali activation and reaction product formation in the mortars. Moreover, due to the lower w/b ratio, the reaction degree of AAS8000–0.5 mortars was lower compared to that of other mixtures, which could contribute more mass gain after exposed to alkaline solution. As the alkaline content of mortars with different w/b ratio is same, if the reaction degree of aggregate is higher, then the reaction degree of binder is lower. For AAS8000–0.8 mortars, the combination of continued activation of unreacted slag and formation and water uptake of ASR gel led to the biggest mass gain in all samples.

3.2.4. Microstructure and chemical composition

Representative backscatter electron micrographs (BSE) of polished samples with different w/b ratios after 80 days exposure is given in Fig. 16. ASR products have formed in all samples and also extruded into the matrix and filled up the cracks in AAS8000–0.6, AAS8000–0.7 and AAS8000–0.8 mortars. Nevertheless, there is an obvious gap in the ASR products vein of AAS8000–0.5 mortars, which is most probable due to the viscosity of ASR products in AAS8000–0.5 is relatively lower compared to those in other mortars. As discussed in Section 3.1.4, the viscosity of ASR products is largely dependent on its chemical composition, and the viscosity of ASR products with low calcium and higher alkali content is low [74,75,82,83]. The EDS results shown in Fig. 17 indicates that AAS8000–0.5 has relatively higher Na and lower Ca content than that of other samples, whereas the calcium content of ASR products in AAS8000–0.8 mortars is higher and Na content lowers. In that case, the viscosity of ASR products in AAS8000–0.8 mortars is generally higher, and more products contribute to the development of expansion rather than flow out, which might partly explain that why the

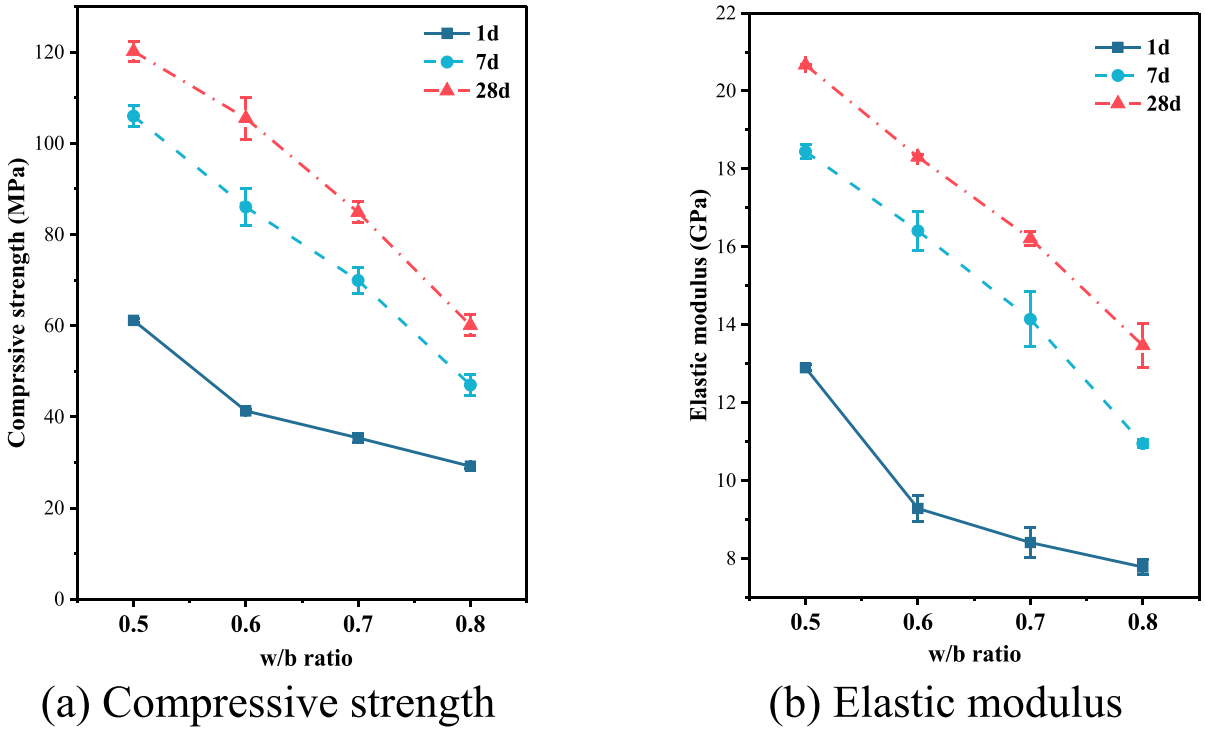

Fig. 11. Mechanical properties development of the AAS8000 mortars with different w/b ratios.

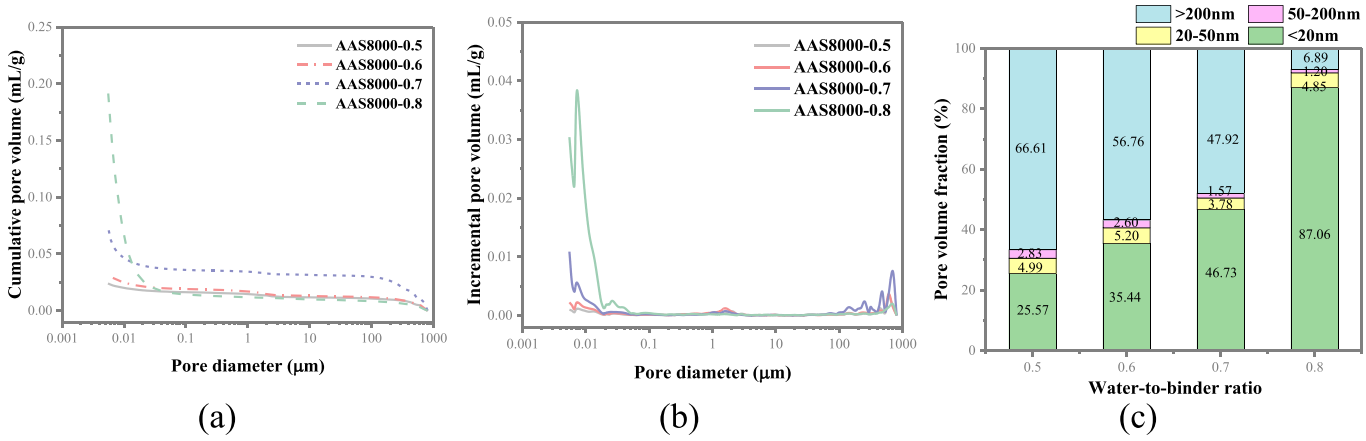

Fig. 12. Pore structure of the AAS8000 pastes with different w/b ratios.

macro-expansion of AAS8000–0.8 mortars is highest.

In additions, it is worth noting that it is easy to find the crystallize ASR products with well-defined texture in AAS8000–0.8 mortars as shown in Fig. 18, indicating a higher crystallinity of ASR products in AAS8000–0.8 mortars. This is consistent with the EDS analysis results and the previous study [77], which reported that crystalline ASR products had a lower Na/K ratio than amorphous one. Since the crystallization pressure favors the stress generation and expansion development [76,77], such high crystallinity could also play a partial role in the larger expansion of AAS8000–0.8 given in Fig. 13.

3.3. Further discussion

Based on the above-mentioned results and analysis, we know the variations of slag fineness and w/b ratio could have a significant influence on the ASR and development of ASR-induced expansion. According to the expansion hypothesis for ASR gel in previous studies [13,19,84,85], the development of ASR-induced expansion could be separated into three distinct stages: early-age reaction, early-stage expansion, and late-stage expansion. Therefore, the emphasis is made here to understand the influence of slag fineness and w/b ratio on the ASR-induced expansion in the above three stages with the support of the experimental evidences found in this study. The discussions are also made in comparison to those in AAMs and OPC system in the following sections.

3.3.1. Mechanism of the influence of slag fineness on ASR in AAS mortars

In OPC system, reducing the particle size of SCMs, such as slag and fly ash, can effectively mitigate ASR expansion due to the enhanced pozzolanic effect. However, compared with OPC system, the role of slag fineness in ASR of AAS mortars is more complex, and it seems that there is a "pessimum effect" in the influence of slag fineness on the ASR in AAS mortars. The slag fineness could influence the rate of hydration, porosity, shrinkage, strength, amount of reactive silica in aggregates and chemical composition of ASR products, and a conceptual model is used

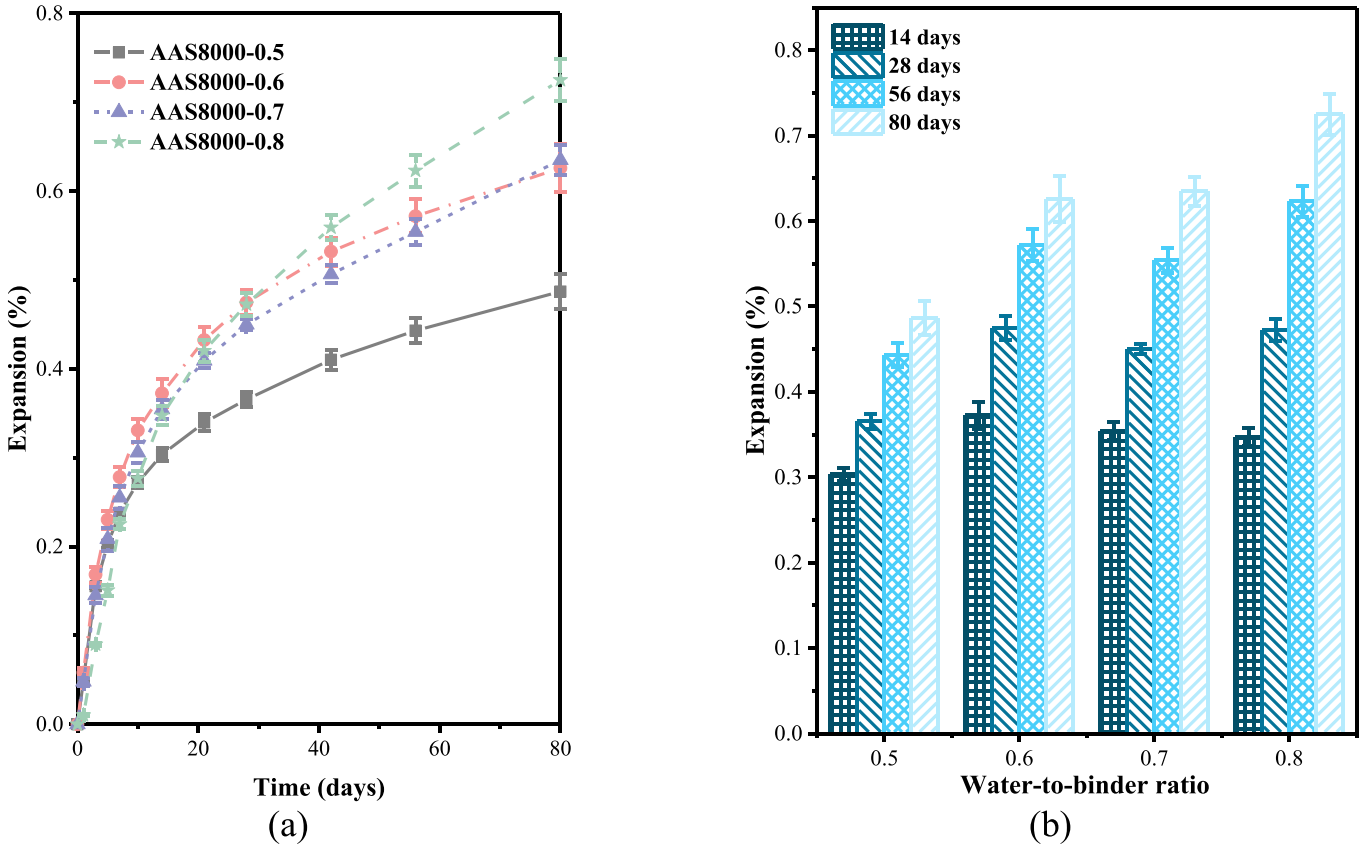

Fig. 13. (a) Expansion development of AAS mortars with w/b ratio; (b) Effect of w/b ratio on the expansion AAS mortars after 14, 28, 56, and 80 days exposure.

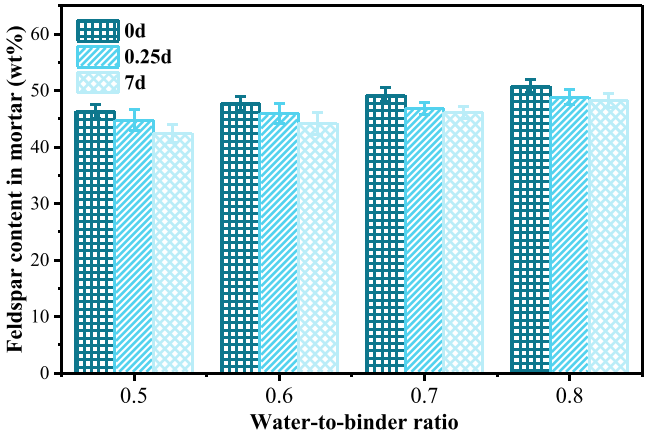

Fig. 14. Feldspar content in AAS mortars with different slag fineness and w/b ratio.

to interpret the phenomenon (Fig. 19).

In the early-age reaction stage, the reaction is governed by the alkali activation of AAS. As mentioned in Section 3.1, with an increase in slag fineness, the porosity of AAS decreased (see Fig. 4), the strength of specimens increased (see Fig. 3) and more reactive silica was kept for ASR (see Fig. 6).

In the early-stage expansion, the difference in the expansion development might be mainly attributed to the reaction kinetics of ASR and microstructures of corresponding specimens. As the alkali content of ASR gel in AAS mortars is relatively high (Fig. 9), the gel formed is easily extruded into the adjacent pores, and the porosity could have great impact on the development of expansion. On one hand, the porosity of

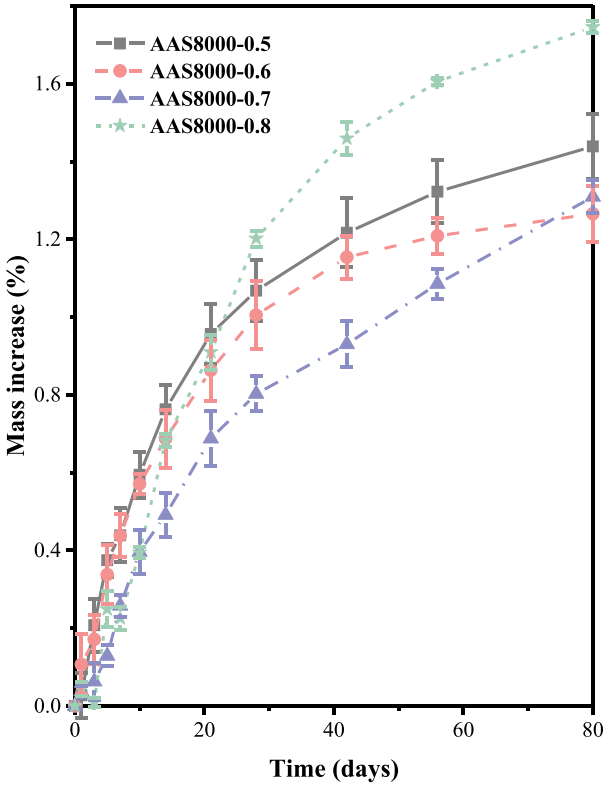

Fig. 15. Effect of w/b ratio on the mass gain of AAS mortars.

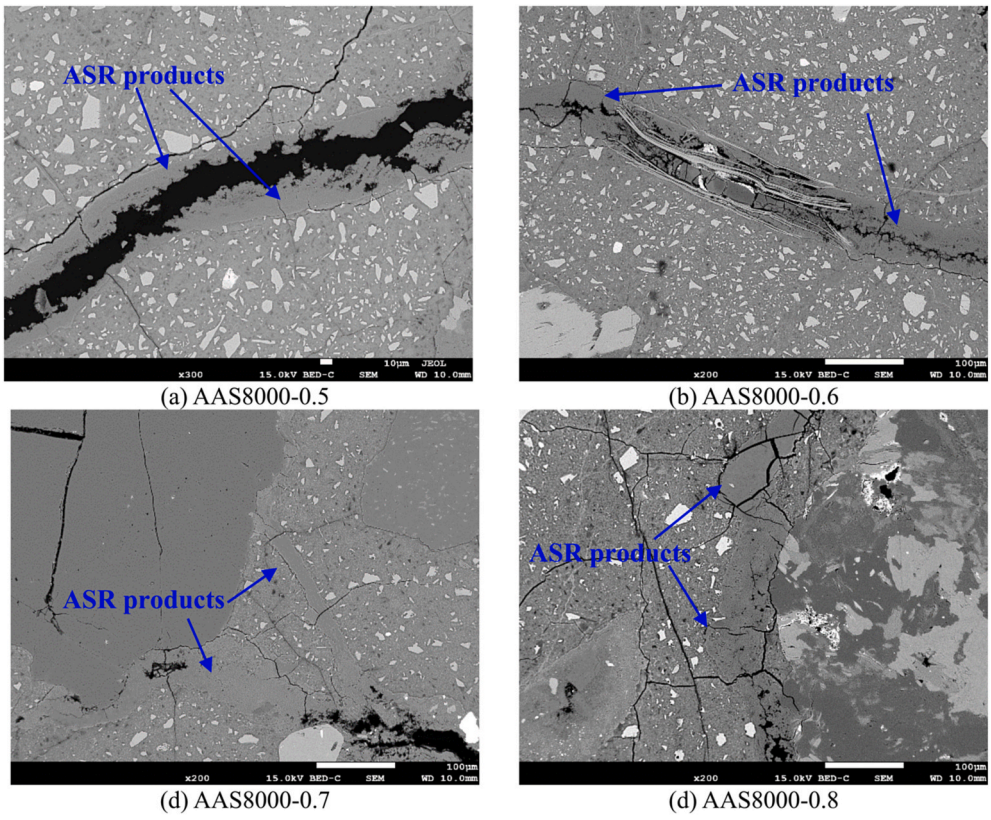

Fig. 16. BSE images of mortar specimens with different w/b ratio after 80 days of AMBT.

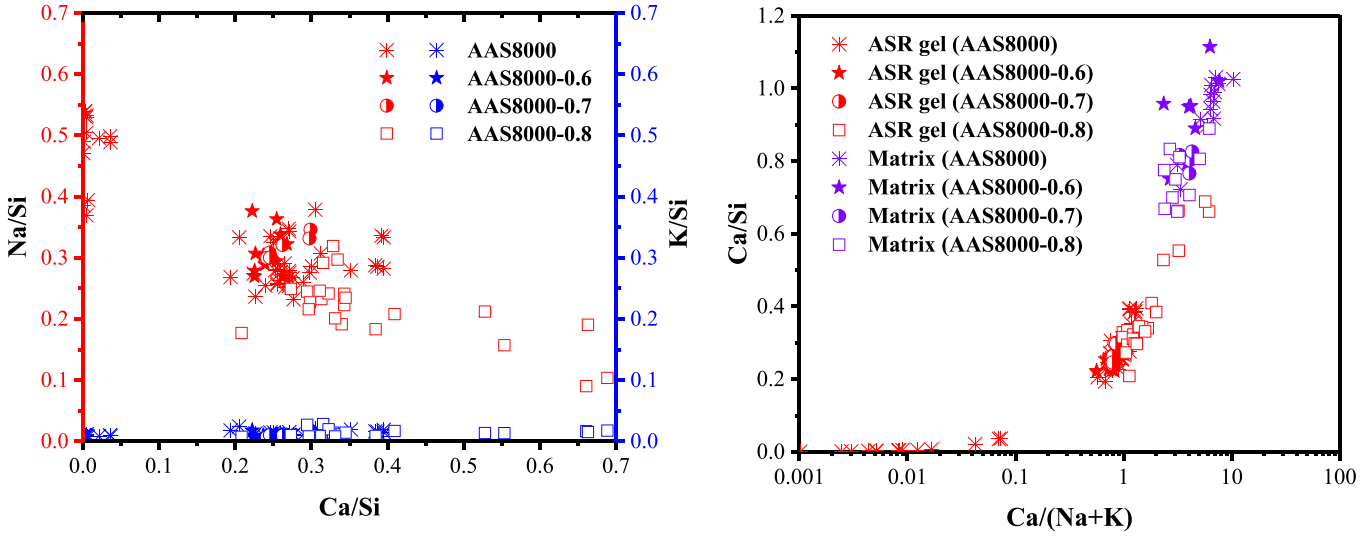

Fig. 17. Chemical composition (atomic ratio) of ASR products and matrix of AAS mortars with different w/b ratio.

AAS specimens decreased with an increase in fineness, and the dense microstructure could not provide the stress-free spaces for the ASR gels. In this case, more ASR gels were restricted in the local area rather than accommodated by pores, which contributed to the development of expansion. Moreover, more reactive silica remained for ASR with increasing slag fineness, which also increase the reaction rate of ASR. In this case, the expansion development of AAS increased with increasing slag fineness. On the other hand, the shrinkage of specimens increased with slag fineness [55,56,86], and the shrinkage could partly offset the expansion and hinder the development of absolute expansion. Furthermore, the shrinkage-induced cracks could provide accommodations for the ASR gels, and even providing paths for the ASR gels to flow out without causing expansion pressure. Besides, due to dense microstructure of AAS, the external alkaline ions in 1 mol/L NaOH solution might need to take time to diffusion front to reach reactive aggregates. Therefore, in the early-expansion stage, the OH^- concentration for ASR might depend on the pore solution of corresponding specimens, and the OH^- concentration would decrease more rapidly with increasing slag

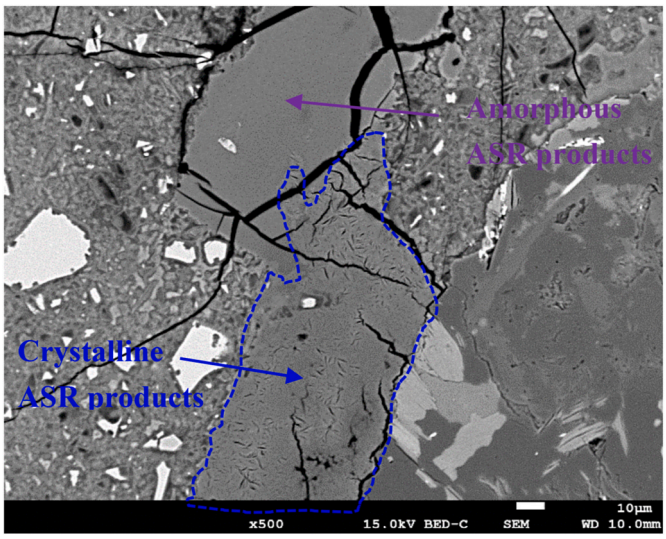

Fig. 18. Amorphous and crystalline ASR products in AAS8000–0.8 mortar specimens.

fineness due to the consumption of OH^- ions in the alkali-activation of AAS. In this case, the rate of ASR in AAS specimens decreased with increasing slag fineness. Consequently, a combination of the above-mentioned reasons results in a "pessimum effect" in the role of slag fineness in ASR-induced development of AAS mortars.

In the late-stage expansion, the difference in the expansion behavior should be dependent on the combination of the development of ASR-induced initial cracks and mechanical properties of matrix. In this stage, the ASR-induced microcracks have extended from the aggregate to matrix. The superior mechanical properties could confine the development of cracks and resultant expansion. New cracks may initiate and propagate when the internal tensile stress caused by ASR gels exceeds the tensile stress of a specimen. Previous studies [53] have suggested that compared with compressive strength, elastic modulus is more important for the development of ASR-induced expansion. As shown in Fig. 3, although the elastic modulus of AAS specimens increased with increasing slag fineness, the increment after 7 days is limited. In this case, the effect of mechanical properties of matrix on the development of expansion in AAS specimens with different slag fineness is also limited. The difference in expansion in this stage is thereby mainly dependent on the development of ASR-induced initial cracks in early-stage expansion. Therefore, the "pessimum effect" of slag fineness runs through the development of ASR-induced expansion in AAS specimens. During the mixture design, this "pessimum effect" should be taken care of and avoided.

3.3.2. *Mechanism of the influence of w/b ratio on ASR in AAS mortars*

Water plays a different role in AAMs compared with that in cementitious materials. Due to the use of alkaline activator, the role of w/b ratio in ASR in AAS mortars becomes more complex. As mentioned above, increasing w/b ratio leads to higher porosity of AAS and thus lower strength of specimens (see Figs. 11 and 12), with increasing amount of reactive silica remained for ASR (see Fig. 14). In this section, a modified conceptual model given in Fig. 20 is used to further interpret the mechanism behind the influence of w/b ratio on the ASR in AAS mortars.

In the early-stage expansion, as the temperature is same in this study, the kinetics is controlled by the alkalinity and amount of reactive silica. With an increase in w/b ratio, the alkalinity of pore solution would decrease, and thereby the reaction kinetics could be decelerated. Moreover, the high porosity could provide more accommodations for the ASR gels without causing expansion pressure, and thereby hinder the development of ASR-induced expansion in AAS specimens with higher w/b ratio. In this case, the development of ASR-induced expansion decreased with increasing w/b ratio. On the other hand, the amount of remained reactive silica increased with increasing w/b ratio, and thereby the reaction kinetic of ASR could be accelerated in the presence of much reactive silica. Furthermore, increasing w/b ratio could result in a lower shrinkage [51,52,87], and the compensation effect in expansion by shrinkage decreased. In this case, the ASR-induced expansion increased with an increase in w/b ratio. Consequently, a combination of the above-mentioned reasons leads to the pessimum effect in the influence of w/b ratio on early-stage ASR expansion in AAS mortars.

In the late-stage expansion, unlike the effect of slag fineness, the elastic modulus of AAS mortars remarkably decreased with increasing w/b ratio (Fig. 11). In that case, the confinement pressure provided by the matrix significantly decreased, and the expansion pressure results from ASR gels could be easily higher than the strength of the matrix and cracks would propagate into the matrix. After matrix cracking, more external alkalis will diffusion into the local area of reactive aggregates, and thereby further accelerate the formation of ASR gels. Moreover, as less reactive silica was dissolved in mortars with higher w/b ratio in the early-age alkali-activation, more reactive silica was kept for ASR rather than participating in the alkali-activation of AAS. Consequently, the ASR-induced expansion increased with increasing w/b ratio in the late-

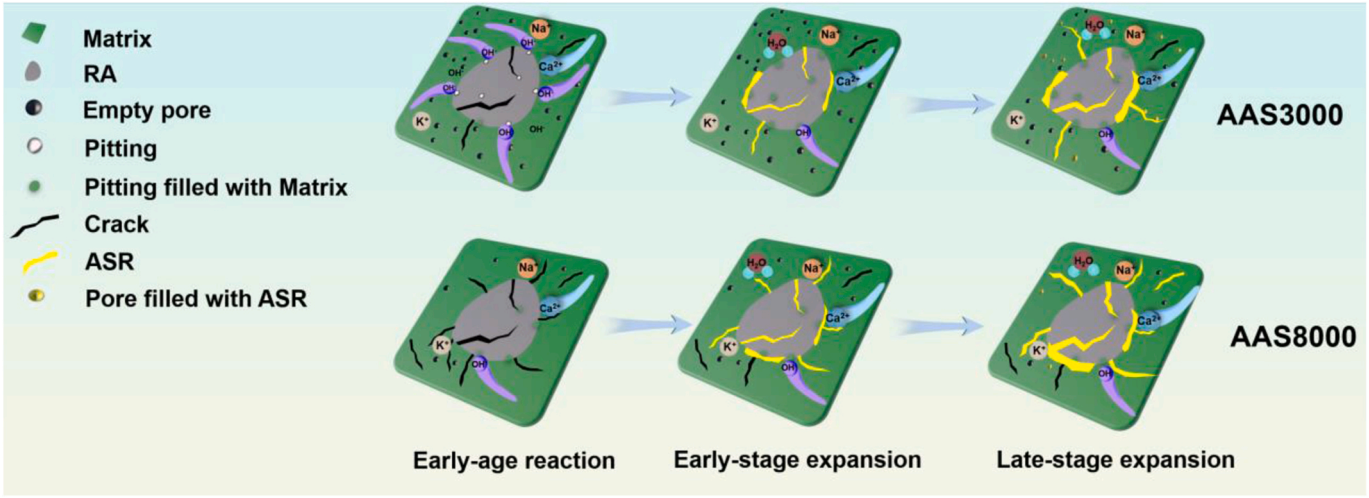

Fig. 19. Schematic representation of ASR in AAS with different slag fineness (w/b = 0.5).

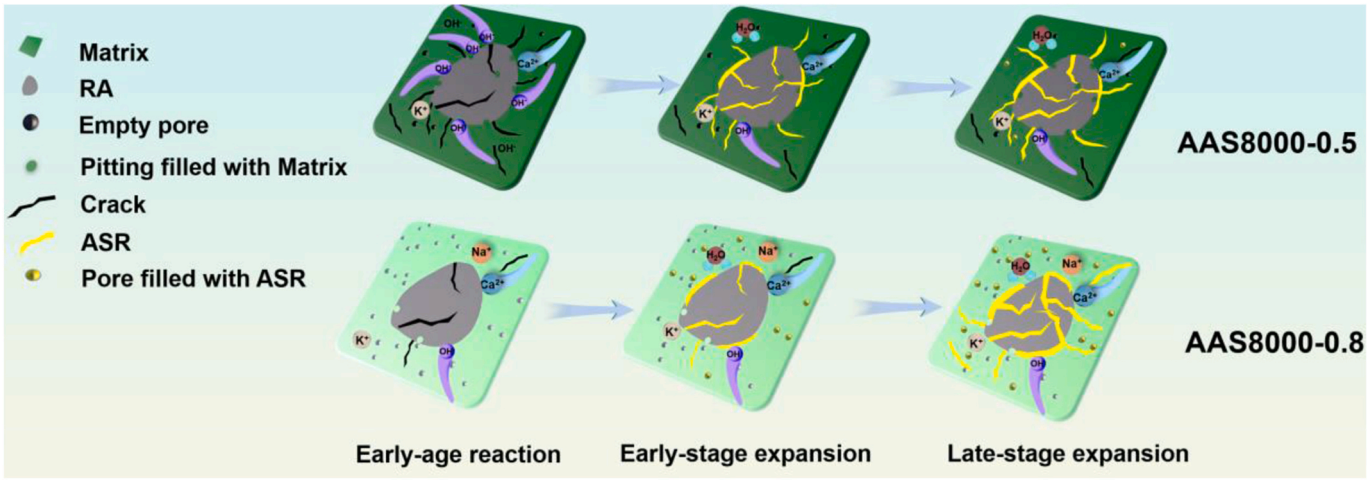

Fig. 20. Schematic representation of ASR in AAS with different w/b ratio.

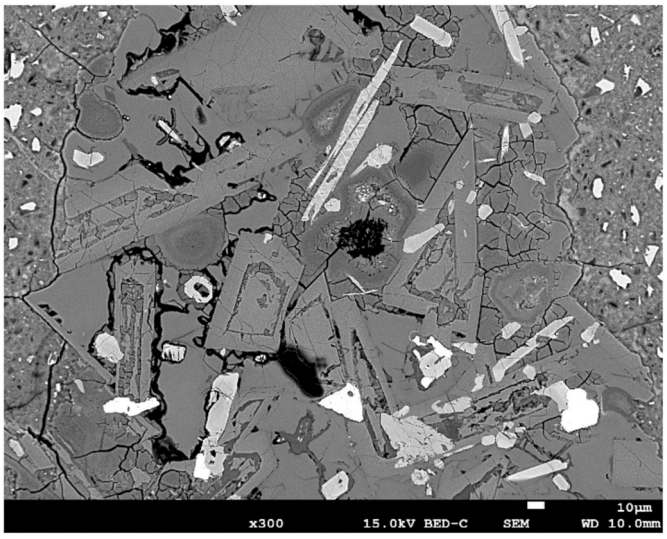

Fig. 21. Degraded reactive aggregate in AAS8000–0.8 mortars.

stage. As shown in Fig. 21, after 80 days exposure to 1 mol/L NaOH solution, the reactive aggregate in AAS8000–0.8 specimen was severely damaged by the ASR, and there are many ASR gels could be observed in the internal part of aggregates.

3.4. Final remarks

In this work, the influence of slag fineness and w/b ratio was respectively investigated at one alkali dosage and silicate modulus, and further studies are needed to clarify the combined or synergistic influence of slag fineness and w/b ratio at different alkali dosage and silicate modulus. Moreover, state-of-the-art methods are desirable to improve the understanding of this phenomenon in a field study. In addition, owing to the variations in chemical composition of precursors from different sources, which might lead to different consequences, it is recommended to further clarify the influence of chemical compositions of precursors on ASR in AAM systems, and thereby further improving the understanding on the mechanism of ASR in AAM systems and providing a suggestion for the following mitigation study as well as designing the mixture for AAMs in practical application.

4. Conclusions and recommendations

This research mainly investigated the effect of slag fineness and water-to-binder ratio on the ASR performance of AAS mortars. Based on the experimental results and discussion, the following conclusions can be drawn.

(1) With an increase in slag fineness, the elastic modulus of AAS pastes slightly increased, while the compressive strength increased in the early-age, and has an optimum range of fineness for the long-term strength. With an increase in w/b ratio, both the compressive strength and elastic modulus significantly decreased
(2) The expansion of mortars increased first and then decreased with increasing slag fineness, and the AAS4000 mortars exhibited highest expansion. The expansion of AAS mortars increased first and then decreased in the early-age ($\leq$14 days), while the expansion of AAS mortars increased with the increasing of w/b ratio in the later-age (>14 days).
(3) The mass gain of AAS mortars increased with increasing slag fineness. The mass gain of AAS8000 mortars was higher than that of AAS8000–0.6 and AAS8000–0.7 mortars, and the mass gain of AAS8000–0.8 mortars were highest in all samples in the later-stage.
(4) The cracks could be observed on the surface on all samples, while AAS6000 and AAS8000 exhibited more visible cracking than samples with different slag fineness. However, the crack width of AAS8000 mortars were the biggest, while AAS8000–0.8 mortars exhibited the lowest crack width due to high self-healing effect in samples with different w/b ratio.
(5) The SEM/EDS analysis illustrated that ASR products could be easily observed in all samples, and it is easy to find the ASR products in all samples. The calcium content of ASR products in AAS4000 mortars was higher than that of samples with different slag fineness, while the sodium content was higher in AAS6000 and AAS8000 mortars. The sodium content in AAS8000 is relatively higher than that of samples with different w/b ratio, while

the calcium content of ASR products in AAS8000–0.8 mortars is higher. Besides, the crystallinity of ASR products in AAS8000–0.8 mortars is high.

(6) For the first time, the influence of slag fineness and w/b ratio on ASR performance were investigate and interpreted, which could further bridge the knowledge gap and further clarify the ASR mechanism in AAMs system.

Based on the data obtained from this study, some recommendations could also be given for the mixture design of AAMs and directions of future studies. Due to the specific mechanism of ASR in AAMs system, if the workability can satisfy the requirements and there is no particular requirement on the mechanical properties or reaction speed, it is recommended to decrease the w/b ratio of mixture, and use the coarser precursors. Because the finer precursor could increase the risk of ASR, shrinkage and cost.

Furthermore, it recommended to further clarify the influence of chemical compositions of precursors on ASR in AAM systems at different alkali dosage and silicate modulus, and providing suggestions for the following mitigation study as well as optimizing the mixture for AAMs in practical application.

CRediT authorship contribution statement

Wei Wang: Writing – review & editing, Writing – original draft, Validation, Resources, Methodology, Investigation, Funding acquisition, Formal analysis, Data curation, Conceptualization. **Shizhe Zhang:** Writing – review & editing, Investigation, Formal analysis. **Yamei Zhang:** Writing – review & editing, Supervision, Methodology, Investigation, Formal analysis, Conceptualization. **Takafumi Noguchi:** Writing – review & editing, Supervision, Project administration, Conceptualization. **Ippei Maruyama:** Writing – review & editing, Visualization, Supervision, Methodology.

Declaration of competing interest

The authors declare that they have no known competing financial interests or personal relationships that could have appeared to influence the work reported in this paper.

Acknowledgements

A part of the research is from the Fundamental Research Funds for the Central Universities (the grant number RF1028623196), and the Japan Society for the Promotion of Science (the grant number 18H03803).

Appendix A. Appearance of the pastes after sealed curing

As shown in Fig. A1, there are many map-cracks on the surface of AAS8000 specimens after 28 days sealed curing, which should be caused by the shrinkage of AAS.

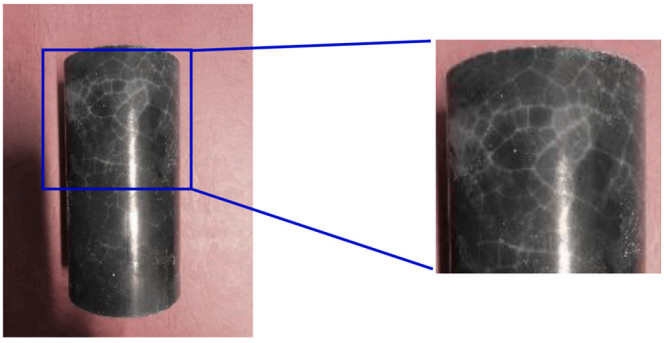

Fig. A1. Appearance of the AAS8000 paste specimen after 28d sealed curing.

Appendix B. Visual inspection of mortar bar specimens subjected to 1N NaOH solution

As shown in Fig. A2, the appearance of the specimens after immersed in 1N NaOH for 21 days at 80 °C were taken and compared. It can be seen that the AAS3000 mortar specimens exhibited minor cracks on the surface, while the AAS4000, AAS6000 and AAS8000 displayed more visible cracking. In addition, there are some white substances precipitated on the cracks, which suggested these specimens suffered from the ASR-induced expansion. Furthermore, the width and number of cracks in AAS6000 and AAS8000 are bigger than that of AAS4000 and AAS3000, which is inconsistent with the expansion results in Section 3.1.2. On the one hand, this phenomenon might be a result of the differences of the properties of ASR gel generated in the corresponding specimens, which is further discussed in Section 3.1.4. On the other hand, the noticeable cracks of AAS6000 and AAS8000 may be owing to a combination of ASR and shrinkage. The high shrinkage of AAS6000 and AAS8000 lead to the micro-cracks in the specimens and provide the convenience for the flow out of ASR products. In that case, some portion of the ASR products could flow out along the shrinkage-induced cracks without further causing expansion pressure, and thereby the expansion rate decreases and plateaued quickly. Therefore, there is a “pessimum effect” of slag fineness on the development of ASR-induced expansion.

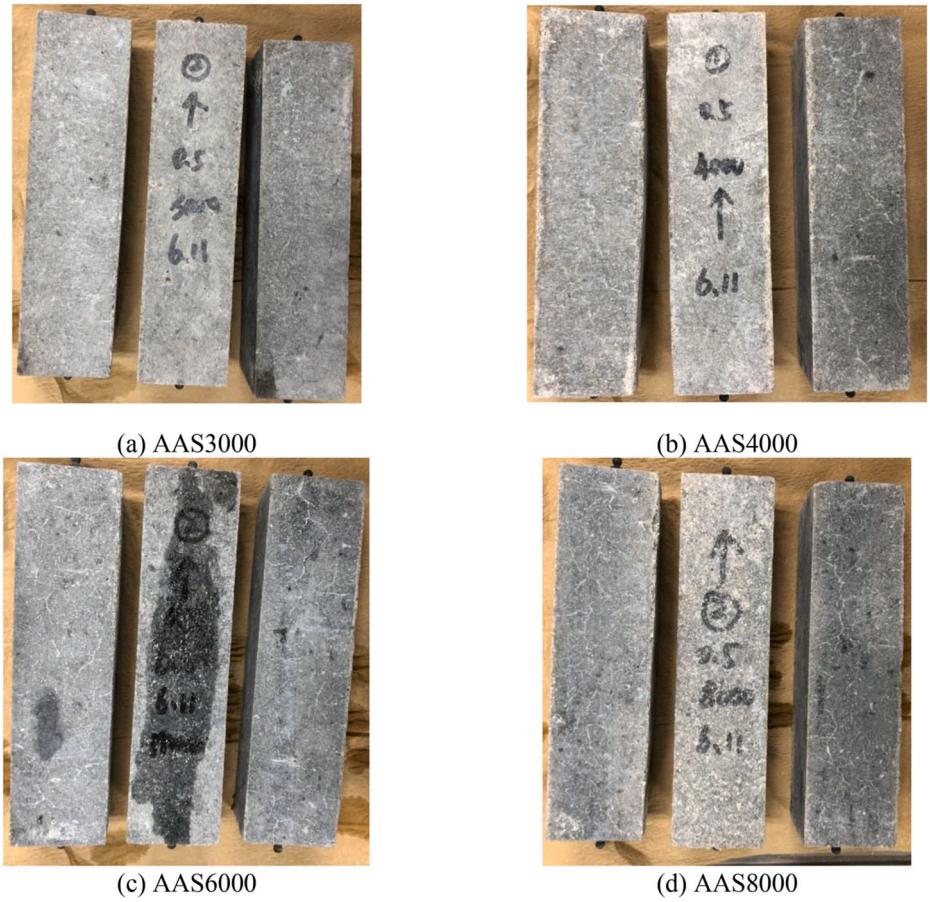

Fig. A2. Visual inspection of AAS mortars with different GGBFS particle size after immersion in 1N NaOH for 21 days.

As shown in Fig. A3, the appearance of the specimens after immersed in 1N NaOH for 21 days at 80 °C were taken and compared. The images show that many cracks could be observed in the surface of all samples. However, it is interesting to find that crack width of AAS8000–0.5 mortars is the biggest, while AAS8000–0.8 mortars exhibited the lowest crack width, which is conserve with the expansion results given in Fig. 12. This phenomenon could be as a result of the higher shrinkage of AAS8000–0.5 mortars. During the compressive strength test, compared with AAS6000, the decreased strength of AAS8000 also suggested this point, and obvious shrinkage cracks could be observed on the surfaces of the corresponding pastes. Therefore, the cracks on the surface of AAS8000–0.5 mortars may be a combination results of shrinkage and expansion. For AAS8000–0.8 mortars, the lowest crack width might be attributed to the self-healing effect caused by the further activation of unreacted binder in alkaline solution. Therefore, the crack width should not be a sole parameter for evaluating the damage degree of the ASR, it needs to be used in conjunction with other methods.

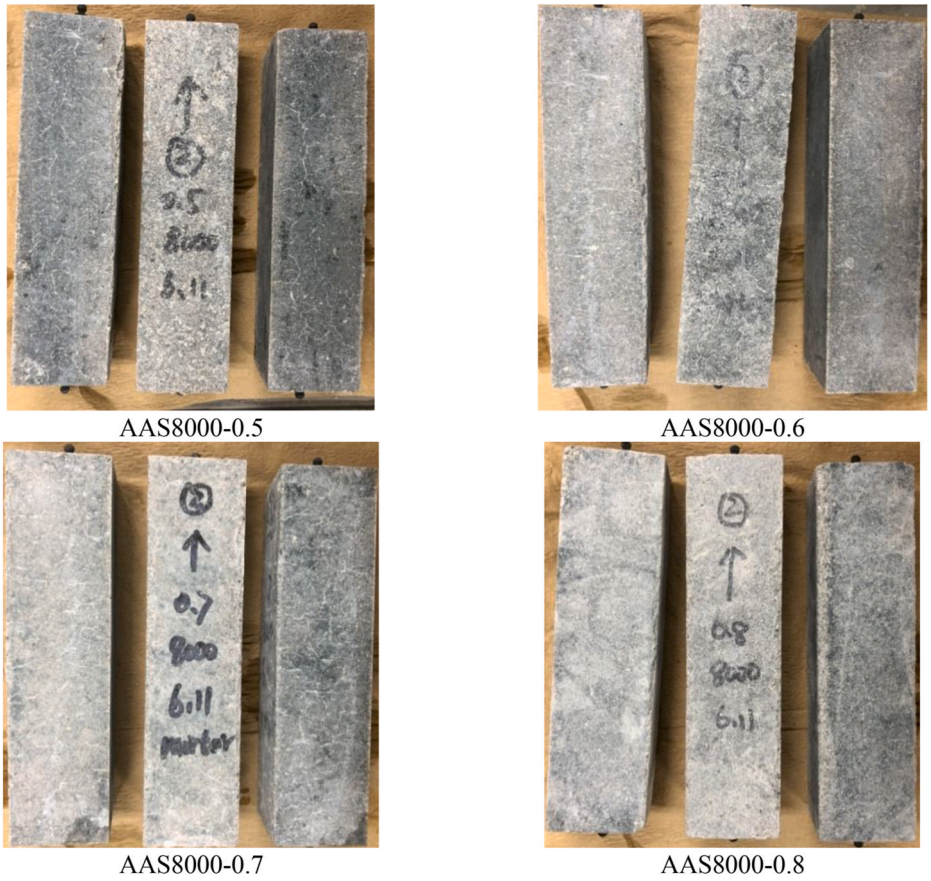

Fig. A3. Visual inspection of AAS mortars after immersion in 1N NaOH for 21 days.

Data availability

Data will be made available on request.

References

[1] C. Shi, A.F. Jiménez, A. Palomo, New cements for the 21st century: the pursuit of an alternative to Portland cement, Cement Concr. Res. 41 (2011) 750–763, https://doi.org/10.1016/j.cemconres.2011.03.016.
[2] J.L. Provis, Alkali-activated materials, Cement Concr. Res. 114 (2018) 40–48, https://doi.org/10.1016/j.cemconres.2017.02.009.
[3] C. Shi, D. Roy, P. Krivenko, Alkali-activated Cements and Concretes, CRC press, 2003.
[4] F. Pacheco-Torgal, J. Labrincha, C. Leonelli, A. Palomo, P. Chindaprasit, Handbook of Alkali-Activated Cements, Mortars and Concretes, Elsevier, 2014.
[5] Y. Ding, J.-G. Dai, C.-J. Shi, Mechanical properties of alkali-activated concrete: a state-of-the-art review, Construct. Build. Mater. 127 (2016) 68–79.
[6] S. Aydın, B. Baradan, Mechanical and microstructural properties of heat cured alkali-activated slag mortars, Mater. Des. 35 (2012) 374–383.
[7] D.L.Y. Kong, J.G. Sanjayan, Effect of elevated temperatures on geopolymer paste, mortar and concrete, Cement Concr. Res. 40 (2010) 334–339.
[8] T. Bakharev, J.G. Sanjayan, Y.-B. Cheng, Sulfate attack on alkali-activated slag concrete, Cement Concr. Res. 32 (2002) 211–216.
[9] T. Bakharev, J.G. Sanjayan, Y.-B. Cheng, Resistance of alkali-activated slag concrete to acid attack, Cement Concr. Res. 33 (2003) 1607–1611.
[10] T. Bakharev, J.G. Sanjayan, Y.B. Cheng, Resistance of alkali-activated slag concrete to alkali-aggregate reaction, Cement Concr. Res. 31 (2001) 331–334, https://doi.org/10.1016/S0008-8846(03)00125-X.
[11] R. Tänzer, Y. Jin, D. Stephan, Effect of the inherent alkalis of alkali activated slag on the risk of alkali silica reaction, Cement Concr. Res. 98 (2017) 82–90, https://doi.org/10.1016/j.cemconres.2017.04.009.
[12] Z. Shi, C. Shi, S. Wan, Z. Zhang, Effects of alkali dosage and silicate modulus on alkali-silica reaction in alkali-activated slag mortars, Cement Concr. Res. 111 (2018) 104–115, https://doi.org/10.1016/j.cemconres.2018.06.005.
[13] W. Wang, T. Noguchi, I. Maruyama, Mechanism understanding of alkali-silica reaction in alkali-activated materials system, Cement Concr. Res. 156 (2022) 106768, https://doi.org/10.1016/j.cemconres.2022.106768.
[14] W. Wang, T. Noguchi, I. Maruyama, Mitigation effect of lithium nitrate on the alkali-silica reaction in alkali-activated slag mortars, Cem. Concr. Compos. 130 (2022) 104532, https://doi.org/10.1016/j.cemconcomp.2022.104532.
[15] T.E. Stanton, Expansion of Concrete through Reaction between Cement and Aggregate, Transactions of the American Society of Civil Engineers, 1942, https://doi.org/10.1061/taceat.0005540.
[16] F. Rajabipour, E. Giannini, C. Dunant, J.H. Ideker, M.D.A. Thomas, Alkali-silica reaction: current understanding of the reaction mechanisms and the knowledge gaps, Cement Concr. Res. 76 (2015) 130–146, https://doi.org/10.1016/j.cemconres.2015.05.024.
[17] J. Lindgård, Ö. Andiç-Çakir, I. Fernandes, T.F. Rønning, M.D.A. Thomas, Alkali-silica reactions (ASR): literature review on parameters influencing laboratory performance testing, Cement Concr. Res. 42 (2012) 223–243, https://doi.org/10.1016/j.cemconres.2011.10.004.
[18] F. Puertas, M. Palacios, A. Gil-Maroto, T. Vázquez, Alkali-aggregate behaviour of alkali-activated slag mortars: effect of aggregate type, Cem. Concr. Compos. 31 (2009) 277–284, https://doi.org/10.1016/j.cemconcomp.2009.02.008.
[19] Y. Kawabata, C. Dunant, K. Yamada, K. Scrivener, Impact of temperature on expansive behavior of concrete with a highly reactive andesite due to the alkali–silica reaction, Cement Concr. Res. 125 (2019) 105888, https://doi.org/10.1016/j.cemconres.2019.105888.
[20] B. Li, L. Baingam, K. Kurumisawa, T. Nawa, L. XiaoZhou, Micro-mechanical modelling for the prediction of alkali-silica reaction (ASR) expansion: influence of curing temperature conditions, Construct. Build. Mater. 164 (2018) 554–569, https://doi.org/10.1016/j.conbuildmat.2018.01.007.
[21] F. Golmakani, R.D. Hooton, Impact of pore solution concentration on the accelerated mortar bar alkali-silica reactivity test, Cement Concr. Res. 121 (2019) 72–80, https://doi.org/10.1016/j.cemconres.2019.02.008.
[22] B. Fournier, M.-A. Bérubé, Alkali-aggregate reaction in concrete: a review of basic concepts and engineering implications, Can. J. Civ. Eng. 27 (2000) 167–191, https://doi.org/10.1139/l99-072.
[23] I. García-Lodeiro, A. Palomo, A. Fernández-Jiménez, Alkali-aggregate reaction in activated fly ash systems, Cement Concr. Res. 37 (2007) 175–183, https://doi.org/10.1016/j.cemconres.2006.11.002.

[24] T. Williamson, M.C.G. Juenger, The role of activating solution concentration on alkali-silica reaction in alkali-activated fly ash concrete, Cement Concr. Res. 83 (2016) 124–130, https://doi.org/10.1016/j.cemconres.2016.02.008.
[25] P. Krivenko, R. Drochytka, A. Gelevera, E. Kavalerova, Mechanism of preventing the alkali – aggregate reaction in alkali activated cement concretes, Cem. Concr. Compos. 45 (2014) 157–165, https://doi.org/10.1016/j.cemconcomp.2013.10.003.
[26] Z. Shi, C. Shi, S. Wan, Z. Ou, Effect of alkali dosage on alkali-silica reaction in sodium hydroxide activated slag mortars, Construct. Build. Mater. 143 (2017) 16–23, https://doi.org/10.1016/j.conbuildmat.2017.03.125.
[27] Z. Shi, C. Shi, J. Zhang, S. Wan, Z. Zhang, Z. Ou, Alkali-silica reaction in waterglass-activated slag mortars incorporating fly ash and metakaolin, Cement Concr. Res. 108 (2018) 10–19, https://doi.org/10.1016/j.cemconres.2018.03.002.
[28] Y. Chen, X. Pu, C. Yang, Q. Ding, Alkali aggregate reaction in alkali slag cement mortars, J. Wuhan Univ. Technol.-Materials Sci. Ed. 17 (2002) 60–62.
[29] A. Fernández-Jiménez, F. Puertas, The alkali-silica reaction in alkali-activated granulated slag mortars with reactive aggregate, Cement Concr. Res. 32 (2002) 1019–1024, https://doi.org/10.1016/S0008-8846(01)00745-1.
[30] R. Pouhet, M. Cyr, Alkali-silica reaction in metakaolin-based geopolymer mortar, Mater. Struct. 48 (2015) 571–583, https://doi.org/10.1617/s11527-014-0445-x.
[31] Z. Li, R.J. Thomas, S. Peethamparan, Alkali-silica reactivity of alkali-activated concrete subjected to ASTM C 1293 and 1567 alkali-silica reactivity tests, Cement Concr. Res. 123 (2019) 105796, https://doi.org/10.1016/j.cemconres.2019.105796.
[32] S. Yang, D. Zheng, C.S. Poon, H. Cui, In-situ alkali–silica reaction evolution of lightweight aggregate concretes prepared with alkali-activated cement and ordinary portland cement assessed by X-ray micro computed-tomography, Cem. Concr. Compos. 140 (2023), https://doi.org/10.1016/j.cemconcomp.2023.105108.
[33] W. Wang, I. Maruyama, T. Noguchi, Impact of exposure conditions on alkali-silica reaction in alkali-activated material systems, Cem. Concr. Compos. 153 (2024), https://doi.org/10.1016/j.cemconcomp.2024.105695.
[34] W. Wang, T. Noguchi, A. Tomoyose, Y. Zhang, I. Maruyama, Influence of volcanic glass powder on alkali-silica reaction expansion in alkali-activated slag mortars, Cem. Concr. Compos. 152 (2024), https://doi.org/10.1016/j.cemconcomp.2024.105665.
[35] C. Shi, Z. Shi, X. Hu, R. Zhao, L. Chong, A review on alkali-aggregate reactions in alkali-activated mortars/concretes made with alkali-reactive aggregates, Mater. Struct. 48 (2015) 621–628, https://doi.org/10.1617/s11527-014-0505-2.
[36] W. Wang, T. Noguchi, Alkali-silica reaction (ASR) in the alkali-activated cement (AAC) system: a state-of-the-art review, Construct. Build. Mater. 252 (2020) 119105, https://doi.org/10.1016/j.conbuildmat.2020.119105.
[37] S. Al-Otaibi, Durability of concrete incorporating GGBS activated by water-glass, Construct. Build. Mater. 22 (2008) 2059–2067, https://doi.org/10.1016/j.conbuildmat.2007.07.023.
[38] B. Sun, Y. Sun, G. Ye, G. De Schutter, A mix design methodology of slag and fly ash-based alkali-activated paste, Cem. Concr. Compos. 126 (2022), https://doi.org/10.1016/j.cemconcomp.2021.104368.
[39] N. Li, C. Shi, Z. Zhang, H. Wang, Y. Liu, A review on mixture design methods for geopolymer concrete, Compos. B Eng. 178 (2019), https://doi.org/10.1016/j.compositesb.2019.107490.
[40] S.D. Wang, K.L. Scrivener, P.L. Pratt, Factors affecting the strength of alkali-activated slag, Cement Concr. Res. 24 (1994) 1033–1043, https://doi.org/10.1016/0008-8846(94)90026-4.
[41] X. Dai, S. Aydin, M. Yücel, K. Lesage, G. De Schutter, Influence of water to binder ratio on the rheology and structural Build-up of Alkali-Activated Slag/Fly ash mixtures, Construct. Build. Mater. 264 (2020) 120253, https://doi.org/10.1016/j.conbuildmat.2020.120253.
[42] M. Thomas, The effect of supplementary cementing materials on alkali-silica reaction: a review, Cement Concr. Res. 41 (2011) 1224–1231, https://doi.org/10.1016/j.cemconres.2010.11.003.
[43] H. Kizhakkumodom Venkatanarayanan, P.R. Rangaraju, Decoupling the effects of chemical composition and fineness of fly ash in mitigating alkali-silica reaction, Cem. Concr. Compos. 43 (2013) 54–68, https://doi.org/10.1016/j.cemconcomp.2013.06.009.
[44] A.K. Saha, M.N.N. Khan, P.K. Sarker, F.A. Shaikh, A. Pramanik, The ASR mechanism of reactive aggregates in concrete and its mitigation by fly ash: a critical review, Construct. Build. Mater. 171 (2018) 743–758, https://doi.org/10.1016/j.conbuildmat.2018.03.183.
[45] Japanese Standards Association, Ground Granulated Blast-Furnace Slag for Concrete, 2013.
[46] Z. Shi, C. Shi, R. Zhao, S. Wan, Comparison of alkali–silica reactions in alkali-activated slag and Portland cement mortars, Mater. Struct. 48 (2015) 743–751, https://doi.org/10.1617/s11527-015-0535-4.
[47] Japanese Standards Association, Physical Testing Methods for Cement, 2015.
[48] Japanese Standards Association, Method of Test for Static Modulus of Elasticity of Concrete, 2017.
[49] K. Scrivener, R. Snellings, B. Lothenbach, A practical guide to microstructural analysis of cementitious materials. https://doi.org/10.1201/b19074, 2016.
[50] W. Gardner, The dynamics of capillary flow, Phys. Rev. 17 (1921) 273–283, https://doi.org/10.1103/PhysRev.18.206.
[51] M. Mastali, P. Kinnunen, A. Dalvand, R. Mohammadi Firouz, M. Illikainen, Drying shrinkage in alkali-activated binders – a critical review, Construct. Build. Mater. 190 (2018) 533–550, https://doi.org/10.1016/j.conbuildmat.2018.09.125.
[52] D. Ballekere Kumarappa, S. Peethamparan, M. Ngami, Autogenous shrinkage of alkali activated slag mortars: basic mechanisms and mitigation methods, Cement Concr. Res. 109 (2018) 1–9, https://doi.org/10.1016/j.cemconres.2018.04.004.
[53] A. Mohammadi, E. Ghiasvand, M. Nili, Relation between mechanical properties of concrete and alkali-silica reaction (ASR); a review, Construct. Build. Mater. 258 (2020) 119567, https://doi.org/10.1016/j.conbuildmat.2020.119567.
[54] H. Zhang, J. Xiao, Y. Tang, Z. Duan, C. sun Poon, Long-term shrinkage and mechanical properties of fully recycled aggregate concrete: testing and modelling, Cem. Concr. Compos. 130 (2022) 104527, https://doi.org/10.1016/j.cemconcomp.2022.104527.
[55] D.P. Bentz, G. Sant, J. Weiss, Early-age properties of cement-based materials. I: influence of cement fineness, J. Mater. Civ. Eng. 20 (2008) 502–508, https://doi.org/10.1061/ASCE0899-1561200820:7502.
[56] H. Justnes, E.J. Sellevold, B. Reyniers, D. Van Loo, A. Van Gemert, F. Verboven, D. Van Gemert, The Influence of Cement Characteristics on Chemical Shrinkage, Autogenous Shrinkage of Concrete, E&FN Spon, London, 1999, pp. 71–80.
[57] I. Maruyama, H. Sugimoto, S. Umeki, R. Kurihara, Effect of fineness of cement on drying shrinkage, Cement Concr. Res. 161 (2022), https://doi.org/10.1016/j.cemconres.2022.106961.
[58] Y. Zhang, K. Wu, Z. Yang, G. Ye, A reappraisal of the ink-bottle effect and pore structure of cementitious materials using intrusion-extrusion cyclic mercury porosimetry, Cement Concr. Res. 161 (2022), https://doi.org/10.1016/j.cemconres.2022.106942.
[59] Y. Ma, G. Wang, G. Ye, J. Hu, A comparative study on the pore structure of alkali-activated fly ash evaluated by mercury intrusion porosimetry, N2 adsorption and image analysis, J. Mater. Sci. 53 (2018) 5958–5972, https://doi.org/10.1007/s10853-017-1965-x.
[60] J. Kaufmann, Characterization of pore space of cement-based materials by combined mercury and wood's metal intrusion, J. Am. Ceram. Soc. 92 (2009) 209–216, https://doi.org/10.1111/j.1551-2916.2008.02834.x.
[61] S. Zhang, Z. Li, B. Ghiassi, S. Yin, G. Ye, Fracture properties and microstructure formation of hardened alkali-activated slag/fly ash pastes, Cement Concr. Res. 144 (2021), https://doi.org/10.1016/j.cemconres.2021.106447.
[62] K. Scrivener, A. Ouzia, P. Juilland, A. Kunhi Mohamed, Advances in understanding cement hydration mechanisms, Cement Concr. Res. 124 (2019), https://doi.org/10.1016/j.cemconres.2019.105823.
[63] T. Ichikawa, Alkali-silica reaction, pessimum effects and pozzolanic effect, Cement Concr. Res. 39 (2009) 716–726, https://doi.org/10.1016/j.cemconres.2009.06.004.
[64] X.X. Gao, S. Multon, M. Cyr, A. Sellier, Alkali-silica reaction (ASR) expansion: pessimum effect versus scale effect, Cement Concr. Res. 44 (2013) 25–33, https://doi.org/10.1016/j.cemconres.2012.10.015.
[65] E. Garcia-Diaz, D. Bulteel, Y. Monnin, P. Degrugilliers, P. Fasseu, ASR pessimum behaviour of siliceous limestone aggregates, Cement Concr. Res. 40 (2010) 546–549, https://doi.org/10.1016/j.cemconres.2009.08.011.
[66] S. Multon, M. Cyr, A. Sellier, P. Diederich, L. Petit, Effects of aggregate size and alkali content on ASR expansion, Cement Concr. Res. 40 (2010) 508–516, https://doi.org/10.1016/j.cemconres.2009.08.002.
[67] C.F. Dunant, K.L. Scrivener, Effects of aggregate size on alkali-silica-reaction induced expansion, Cement Concr. Res. 42 (2012) 745–751, https://doi.org/10.1016/j.cemconres.2012.02.012.
[68] Y. Zuo, M. Nedeljković, G. Ye, Pore solution composition of alkali-activated slag/fly ash pastes, Cement Concr. Res. 115 (2019) 230–250, https://doi.org/10.1016/j.cemconres.2018.10.010.
[69] A. Vollpracht, B. Lothenbach, R. Snellings, J. Haufe, The pore solution of blended cements: a review, Materials and Structures/Materiaux et Constructions 49 (2016) 3341–3367, https://doi.org/10.1617/s11527-015-0724-1.
[70] R.R. Lloyd, J.L. Provis, J.S.J. Van Deventer, Pore solution composition and alkali diffusion in inorganic polymer cement, Cement Concr. Res. 40 (2010) 1386–1392, https://doi.org/10.1016/j.cemconres.2010.04.008.
[71] S. Song, H.M. Jennings, Pore solution chemistry of alkali-activated ground granulated blast-furnace slag, Cement Concr. Res. 29 (1999) 159–170, https://doi.org/10.1016/S0008-8846(98)00212-9.
[72] F. Puertas, A. Fernández-Jiménez, M.T. Blanco-Varela, Pore solution in alkali-activated slag cement pastes. Relation to the composition and structure of calcium silicate hydrate, Cement Concr. Res. 34 (2004) 139–148, https://doi.org/10.1016/S0008-8846(03)00254-0.
[73] T. Kim, J. Olek, H.G. Jeong, Alkali-silica reaction: kinetics of chemistry of pore solution and calcium hydroxide content in cementitious system, Cement Concr. Res. 71 (2015) 36–45, https://doi.org/10.1016/j.cemconres.2015.01.017.
[74] A. Gholizadeh Vayghan, F. Rajabipour, J.L. Rosenberger, Composition-rheology relationships in alkali-silica reaction gels and the impact on the Gel's deleterious behavior, Cement Concr. Res. 83 (2016) 45–56, https://doi.org/10.1016/j.cemconres.2016.01.011.
[75] A. Gholizadeh-Vayghan, F. Rajabipour, Quantifying the swelling properties of alkali-silica reaction (ASR) gels as a function of their composition, J. Am. Ceram. Soc. 100 (2017) 3801–3818, https://doi.org/10.1111/jace.14893.
[76] A. Leemann, B. Münch, The addition of caesium to concrete with alkali-silica reaction : implications on product identification and recognition of the reaction sequence, Cement Concr. Res. 120 (2019) 27–35, https://doi.org/10.1016/j.cemconres.2019.03.016.
[77] A. Leemann, Z. Shi, J. Lindgård, Characterization of amorphous and crystalline ASR products formed in concrete aggregates, Cement Concr. Res. 137 (2020) 106190, https://doi.org/10.1016/j.cemconres.2020.106190.

[78] M.C. Garci Juenger, H.M. Jennings, Examining the relationship between the microstructure of calcium silicate hydrate and drying shrinkage of cement pastes, Cement Concr. Res. 32 (2002) 289–296.
[79] Y. Li, J. Bao, Y. Guo, The relationship between autogenous shrinkage and pore structure of cement paste with mineral admixtures, Construct. Build. Mater. 24 (2010) 1855–1860, https://doi.org/10.1016/j.conbuildmat.2010.04.018.
[80] T. Aly, J.G. Sanjayan, Effect of pore-size distribution on shrinkage of concretes, J. Mater. Civ. Eng. 22 (2010) 525–532, https://doi.org/10.1061/ASCE0899-1561201022:5525.
[81] I. Garcia-lodeiro, A. Palomo, A. Fernández-jiménez, D.E. Macphee, Compatibility studies between N-A-S-H and C-A-S-H gels . Study in the ternary, Cement Concr. Res. 41 (2011) 923–931, https://doi.org/10.1016/j.cemconres.2011.05.006.
[82] A. Gholizadeh-Vayghan, F. Rajabipour, M. Khaghani, M. Hillman, Characterization of viscoelastic behavior of synthetic alkali–silica reaction gels, Cem. Concr. Compos. 104 (2019) 103359, https://doi.org/10.1016/j.cemconcomp.2019.103359.
[83] A. Gholizadeh-Vayghan, F. Rajabipour, The influence of alkali–silica reaction (ASR) gel composition on its hydrophilic properties and free swelling in contact with water vapor, Cement Concr. Res. 94 (2017) 49–58, https://doi.org/10.1016/j.cemconres.2017.01.006.
[84] C. Dunant, Experimental and Modelling Study of the Alkali-Silica – Reaction in Concrete, 2009, p. 4510.
[85] C.F. Dunant, K.L. Scrivener, Micro-mechanical modelling of alkali-silica-reaction-induced degradation using the AMIE framework, Cement Concr. Res. 40 (2010) 517–525, https://doi.org/10.1016/j.cemconres.2009.07.024.
[86] I. Maruyama, H. Sugimoto, S. Umeki, R. Kurihara, Effect of fineness of cement on drying shrinkage, Cement Concr. Res. 161 (2022), https://doi.org/10.1016/j.cemconres.2022.106961.
[87] F. Collins, J.G. Sanjayan, Effect of pore size distribution on drying shrinkage of alkali-activated slag concrete, Cement Concr. Res. 30 (2000) 1401–1406.